NOVA SCHOOL OF SCIENCE & TECHNOLOGY

DEPARTMENT OF PHYSICS

DANIEL DE VASCONCELOS QUELHAS BRAGA

Bachelor of Science in Biomedical Engineering

ANALYSIS OF TRACE ELEMENTS IN HUMAN SOFT TISSUES FROM CANCEROUS PATIENTS USING X RAY FLUORESCENCE

MASTER IN BIOMEDICAL ENGINEERING

NOVA University Lisbon
November, 2021

NOVA SCHOOL OF SCIENCE & TECHNOLOGY

DEPARTMENT OF PHYSICS

ANALYSIS OF TRACE ELEMENTS IN HUMAN SOFT TISSUES FROM CANCEROUS PATIENTS USING X RAY FLUORESCENCE

DANIEL DE VASCONCELOS QUELHAS BRAGA

Bachelor of Science in Biomedical Engineering

Adviser: Prof. Dr. António Alberto Dias
Auxiliary Professor, NOVA School of Science and Technology

Co-adviser: Prof. Dr. Alda Sofia Pessanha de Sousa Moreno
Auxiliary Researcher, NOVA School of Science and Technology

Examination Committee:

Chair: Prof. Dr. Carla Maria Pereira Quintão
Auxiliary Professor, NOVA School of Science and Technology

Rapporteur: Prof. Dr. Ana Guilherme Buzanich
Scientist, BAM – Bundesanstait fur Materialforschung und -prufung

Adviser: Prof. Dr. António Alberto Dias
Auxiliary Professor, NOVA School of Science and Technology

MASTER IN BIOMEDICAL ENGINEERING

NOVA University Lisbon
November, 2021

Analysis of Trace Elements in Human Soft Tissues from Cancerous Patients Using X Ray Fluorescence

To Manuel.

Acknowledgements

This dissertation marks the end of perhaps the most important 5 year period of my life until now. I will do my best to express a few words of gratitude to the people that joined me in my journey and helped me though it.

I will start with the people without whom this work wouldn't have been possible, and it wouldn't be fair if the first people I thanked weren't Professor António Dias and Professor Sofia Pessanha. For their guidance and everything they taught me, for their limitless and continuous availability and will to help. I will forever be grateful to you.

I would also like to thank Professor Sofia Barbosa, for taking the time introducing me to R, and sharing some of her scripts. I will certainly carry the skills I acquired and applied to this work thanks to her teachings. Dr. José Vilchéz and Dr. Carlos Montenegro from the Pathological Anatomy unit of the Centro Hospitalar Barreiro Montijo, for their efforts in making this collaboration possible and sharing the samples used in this work. Ana Ensina, Patrícia Carvalho, Alexandre Veiga, for providing mappings, samples and information that allowed my work to move forward in a time when the pandemic pushed everything backwards.

Now, the people who helped me get to this final step. First of all obviously Sofia Marques, thank you for being my number one fan and always putting up with my nonsense. To all my friends, I can not express how grateful I am to have met you. To thank you all properly would require a dissertation of its own, so I'll leave it for another occasion. And finally, the biggest words of gratitude go out to my family. They are the ones who made it possible for me to study what I love, made my victories their own and supported me no matter what. Thank you to all of those who watched me begin and end this journey, and to my grandfather Manuel who wished he could have done.

"For me, I am driven by two main philosophies: know more today about the world than I knew yesterday and lessen the suffering of others. You'd be surprised how far that gets you."
(Neil deGrasse Tyson)

Abstract

Cancer is one of the largest causes of death globally, causing millions of deaths each year. Its better understanding is crucial for the development and improvement of treatments.

In recent years, trace elements have been used as biomarkers for carcinogenesis, but the number of studies on this subject is small due to the difficulty in obtaining a statistically meaningful number of samples.

The use of formalin fixed paraffin embedded (FFPE) samples, which are widely available in hospitals, is a potential solution to the scarcity of samples, but their analysis is harder due to the presence of the paraffin.

In this work, a total of 58 normal-tumor pairs of FFPE samples were analyzed (30 pairs of colon samples and 28 of breast samples) with the goal of developing a method capable of overcoming the difficulties imposed by the paraffin, and producing an accurate comparison between the concentration of trace elements in normal and tumor tissue.

The samples were analyzed with the M4 TORNADO μXRF spectrometer. An image processing tool was developed in R to select the best areas on the sample to extract the spectra. The quantitative analyses was done with the Fundamental Parameters Method with the use of two matrices, one for colon (38% H, 11% C, 3% N and 46% O) and one for breast (39% H, 22% C, 2% N and 35% O). The matrix compositions were determined based on the mean Z of the FFPE samples for each organ, obtained through the determination of the Compton-to-Rayleigh ration in the spectra and comparison with a reference curve.

The statistical analysis was performed in R. The Shapiro-Wilk test was applied to test the normality of the distributions of each element in each type of tissue. To compare the normal and tumor distributions of each element, two non-parametric tests were used: the Kruskal-Wallis test and the Wilcoxon test.

The elements that were found to be potential tumor biomarkers were P and S in colon, and P, S, Ca, Fe and Zn in breast. In colon, significant changes were also found in Fe and Ni, but more research is needed to conclude about their involvement in carcinogenesis.

Keywords: Cancer, Colon, Breast, μXRF, Trace Elements, Fundamental Parameters

Resumo

O cancro é uma das maiores causas de morte globalmente, causando milhões de mortes anualmente. O conhecimento acerca deste grupo de doenças é crucial para o desenvolvimento e melhoramento dos tratamentos. Recentemente, os elementos de traço têm sido utilizados como biomarcadores da carcinogénese, mas o número de estudos realizados sobre este assunto é reduzido devido às dificuldades na obtenção de um número significativo de amostras. O uso de amostras fixadas em formol e embebidas em parafina (FFPE), que estão disponíveis em grande número nos hospitais, são uma potencial solução para a escacez de amostras, no entanto a sua análise é de maior dificuldade devido a presença da parafina.

Neste trabalho, 58 pares normal-tumor de amostras FFPE foram analisadas (30 pares de cólon e 28 de mama) com o objetivo de desenvolver um método capaz de ultrapassar as dificuldades impostas pela parafina e encontrar diferenças na concentração dos elementos de traço em tecido normal e tumoral. As amostras foram analisadas com o M4 TORNADO μXRF spectrometer. Foi desenvolvida em R uma ferramenta de processamento de imagem para selecionar as melhores áreas da amostra para a extração dos espectros. A análise quantitativa foi realizada com o método dos Parâmetros Fundamentais através do uso de duas matrizes, uma para cólon (38% H, 11% C, 3% N e 46% O), e outra para mama (39% H, 22% C, 2% N e 35% O). As composições das matrizes foram determinadas com base no Z médio das amostras. A análise estatística foi realizada em R. Foi utilizado o teste Shapiro-Wilk para averiguar a normalidade das distribuições de cada elemento em cada tipo de tecido. Para comparar as distribuições de cada elemento em tecido normal e tumoral foram utilizados dois testes não paramétricos: Kruskal-Wallis e Wilcoxon.

Os resultados mostram que os elementos com potencial para serem utilizados como biomarcadores são P e S no cólon, e P, S, Ca, Fe e Zn na mama. No cólon,também foram encontradas diferenças significativas entre tecido normal e tumoral nas concentrações dos elementos Fe e Ni, mas é necessária mais pesquisa para se poder tirar conclusões.

Palavras-chave: Cancro, Colon, Mama, μXRF, Elementos de Traço, Parâmetros Fundamentais

Contents

List of Figures

List of Tables

Abbreviations

μEDXRF micro Energy Dispersive X Ray Fluorescence xi, 6, 7, 12, 33, 54

CRM Certified Reference Materials xiv, 8, 9, 20

EDXRF Energy Dispersive X Ray Fluorescence 6, 7, 9, 19, 28

FFPE Formalin Fixed Paraffin Embedded 1, 11, 12, 14, 21, 24, 26, 29, 30, 31, 54, 55

ICP-OES Inductively Coupled Plasma Optical Emission Spectrometry xi, xiv, 11, 12, 20, 24, 33

TXRF Total Reflection X Ray Fluorescence 6, 9

WDXRF Wavelength Dispersive X Ray Fluorescence 6

XRF X Ray Fluorescence 3, 4, 7, 8, 9, 13

1

Introduction

This chapter contains the motivation behind this work, the main goals aimed to be accomplished, a brief explanation of the fundamental concepts regarding this work's theme, and a state of the art section summarizing the findings of other researchers that are relevant to this work.

1.1 Motivation

According to the World Health Organization [2], cancer was responsible for an estimated 9.6 million deaths in 2018, being the second largest cause of death that year.

Cancer is a large group of diseases, and its better understanding is crucial for the improvement of the treatments currently available.

In recent years, trace elements have been used as biomarkers in tumor development, as will be shown in the State of the Art section of this chapter. The number of studies done on this subject is relatively small, and one of the main reasons for that is the difficulty in obtaining a statistically meaningful number of samples, since there must be an informed consent from the patient for the extracted tissue to be used in scientific studies. On top of all the hindering caused by the bureaucracy involved in the acquisition of the tissue, in these types of studies the samples usually undergo some sort of preparation that renders them useless for other types of analysis, which contributes to the scarcity of human tumor tissue samples.

Samples of cancer tissue formalin fixed and paraffin embedded (FFPE) are widely available in hospitals that care for patients suffering from these pathologies. These samples are not often used in these studies because they mustn't be destroyed, and the paraffin makes the analysis more complex, by adding uncertainty in the dark matrix determination.

The adaptation and improvement of the Fundamental Parameter method for the quantification of trace element concentrations in FFPE samples using X Ray Fluorescence might prove to be a valuable asset in this field. It will allow the analysis of samples containing tumorous and normal tissue form the same donor stabilized in paraffin without

any preparation or damage to the samples. This would facilitate the access to samples for trace element analysis, since they can be returned to the institution that provided them in the same conditions as they were before.

With the increase of possible samples to be studied, the statistical validity of the results obtained will improve, and so will the potential number of studies done on the subject, which can be vital for obtaining more knowledge about carcinogenesis.

1.2 Objectives

The main goal of this work is to compare the elemental composition of cancerous and normal tissues form the same donor through the use of X Ray Fluorescence Spectroscopy to gain knowledge and understanding of trace elements as biomarkers for carcinogenesis.

In order for that goal to be accomplished with good results, three other goals must be accomplished first. Those are:

- Analysing the samples fixed in formalin and embedded in paraffin using micro Energy Dispersive X Ray Fluorescence Spectroscopy;
- Overcoming the difficulties in quantification imposed by the presence of paraffin in the samples, more specifically, locating the tissue within the paraffin block in order to improve quantification precision;
- Improving the accuracy of the standardless quantification method through the Fundamental Parameters approach;

1.3 Concepts

1.3.1 Trace Elements

The chemical elements needed in quantities of around 0.01% of the total body composition by weight are commonly referred to as trace elements. They play an important role in several biologic processes, such as enzyme activity and structural functions [3], but they are often linked with toxicity when they exist in quantities that differ from those considered normal [4]. Many links between clinical conditions and the lack of or excessive accumulation of trace elements, and the monitoring of these elements has been an important factor in fighting these type of diseases [5]. The use of more sophisticated spectroscopy techniques has established trace elements as a useful biomarker for several diseases and allowed for studies on their role potential use as biomarkers for carcinogenesis [6].

1.3.2 X Ray Emission

The production of X Rays and the resulting X Ray emission spectrum play a role in the acquisition of an X Ray Fluorescence spectrum, since that is where the process begins.

The X Ray emission spectrum has two prominent features, that both have an impact on the XRF spectrum: the **Continuous Radiation** (*Bremsstrahlung*) and the **Characteristic Radiation**. An example of an X Ray emission spectrum is shown in figure 1.1.

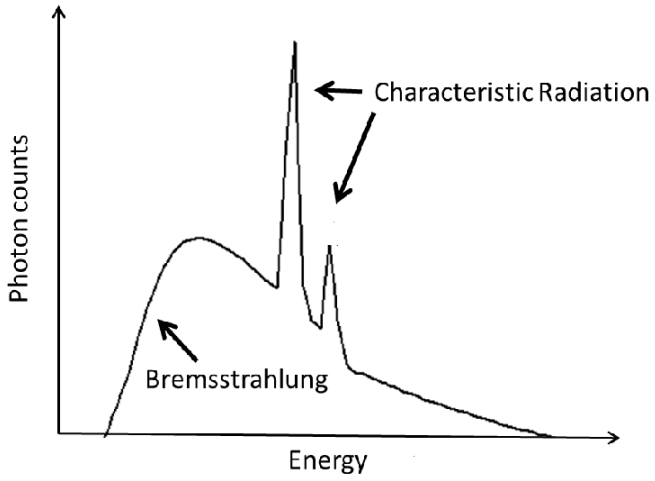

Figure 1.1: X Ray emission spectrum example (adapted from [7]).

1.3.2.1 Continuous Radiation

In the X Ray tube, free electrons are produced in the cathode, through thermionic emission. Those electrons are accelerated to the anode due to the applied voltage. Upon reaching the anode, the electrons interact with the anode's atoms. They are accelerated due to the interaction with the positive electric field of the anode's atoms nucleus. When decelerated, the electrons emit energy under the form of electromagnetic radiation - the *Bremsstrahlung* radiation.

The photons generated through this process are responsible for the continuous component of the X Ray emission spectrum. It is the scattering of these photons in the sample that cause the background in the XRF spectrum [8].

1.3.2.2 Characteristic Radiation

Similarly to what occurs with the continuous radiation, the characteristic Radiation is also caused by interactions of the accelerated electrons with the anode's atoms. However, in this case, the interactions are with the anode's atoms' electrons, rather then their nuclei. The accelerated electrons will cause the ejection of electrons from the inner shells of the anode's atoms, leaving it in an unstable ionized state. One of the electrons from the outer shell will then fill the hole left by the ejected electron, transitioning to the inner shell and emitting an x ray photon with an energy correspondent to that transition.

Since the Characteristic Radiation depends on the element of the anode, and on the transitions that took place to emit it, the photons emitted though this process have discrete and well defined energies which explains the peaks in the X Ray emission spectrum.

In the XRF spectrum, the Compton and Rayleigh scattering of these characteristic photons in the sample gives rise to the most prominent peaks.

1.3.3 Interactions of X Rays With Matter

For the interpretation of the obtained X Ray Fluorescence spectra, it is important to have a basic understanding of the interactions between the incident X Rays and the samples. Given the energy range of X Rays (100 eV to 100 keV), the interactions that take place are those between the X Ray photons and the electrons of the atoms in the sample. The most relevant phenomena are **Compton** scattering, **Rayleigh** scattering and **Photoelectric** absorption [9].

1.3.3.1 Compton and Rayleigh Scattering

In these two scattering phenomena, there is a deflection of the photon upon colliding with the atom's electron. Compton scattering occurs when part of the energy of the incident X Ray photon is transferred to the electron, resulting in a scattered photon with less energy than the incident photon. The energy of the scattered photon is given by equation 1.1:

$$E_{\gamma'} = \frac{E_\gamma}{1 + \frac{E_\gamma}{m_e c^2} \cdot (1 - cos\theta)} \tag{1.1}$$

where $E_{\gamma'}$ is the energy of the scattered photon, E_γ is the energy of the incident photon, m_e is the mass of the electron at rest, c is the speed of light and θ is the scattering angle.

As for Rayleigh scattering, the scattered photon has the same energy as the incident photon. This happens because the electron absorbs the energy of the incident photon and transits to a virtual state. Upon relaxation back to its original state, it emits a photon with the same energy as the incident photon but in a different direction – the scattered photon.

Even though these two interactions do not give rise to fluorescence phenomena, their occurrence generates features in the XRF spectrum, such as the background of the spectrum, resulting from the scattering of the *Bremsstrahlung* radiation, as explained earlier, and also the peaks resulting from the scattering of the characteristic radiation of the X Ray source, which can be useful for quantitative analysis [10–12].

The ratio between Compton and Rayleigh scattering depends on the energy of the photons, the Z of the scatterer (the sample, in the case of XRF spectrometry), and the angle at which the the incident photons interact with the scatterer [8]. This means that for fixed values of and photon energy (which can be defined in XRF spectrometry by fixing the voltage and current of the X Ray tube), the Compton-to-Rayleigh ratio can provide information about the Z of the scatterer [10–12].

Compton scattering is favoured at high energy incident photons, low Z elements and high incidence angles [8], meaning that samples with lower Z should have a higher

Compton-to-Rayleigh ratio, while samples with a higher Z should have a lower Compton-to-Rayleigh ratio.

1.3.3.2 Photoelectric Absorption

Photoelectric absorption occurs when the incident X Ray photon has an energy superior to the binding energy of the electrons from one of the inner shells. This interaction will cause one of those inner shell electrons to be ejected, creating a hole in that shell and leaving the ionized atom in an excited state. The ionized atom will inevitably tend to transition to a more stable state by filling the hole left in the inner shell by the ejected electron with an electron from an outer shell. This can happen through one of two competing processes: **Auger electron emission** or **X Ray fluorescence**.

In Auger electron emission, the filling of the hole in the inner shell by an electron from one of the outer shells is accompanied by the ejection of an electron from the outer shell.

In X Ray fluorescence, the filling of the hole in the inner shell by an electron from one of the outer shells results in the emission of characteristic X Ray photons. The energy of these emitted photons depends on the element and on the energy difference between the two shells involved in the transition of the electron. The emitted characteristic radiation can, therefore, act as a "fingerprint"for the each element and be used effectively to identify those elements in a sample.

The yield for both phenomena in relation to the atomic number of the atom is shown in figure 1.2:

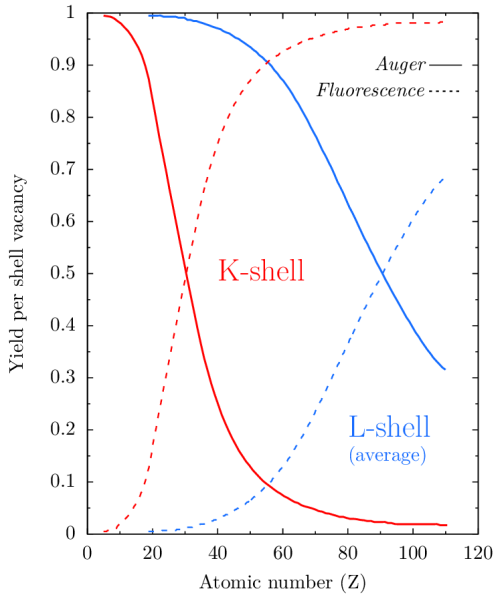

Figure 1.2: Auger and fluorescence yield for different values of Z [13].

In figure 1.2, it can be observed that Auger electron emission is favoured for elements

of low atomic number, while fluorescence becomes dominant for elements of high atomic number.

1.3.4 X Ray Fluorescence Techniques

X Ray Fluorescence Spectroscopy techniques allow for the determination of the elemental structure of a sample in a non-destructive manner, meaning that it is possible to study the same sample more than once without damaging it. They provide data that is simple to interpret and the possibility for portable setups.

The general X Ray Fluorescence Spectroscopy setup includes an X Ray source, a sample, and a detector. The primary X Ray photons are produced in the detector and are directed towards the sample. The fluorescence photons resultant of the interactions between the primary X Ray photons and the sample are detected by the detector.

X Ray Fluorescence techniques can be split into:

- Energy Dispersive X Ray Fluorescence (EDXRF), where energies are all measured simultaneously and discriminated in the detector.
- Wavelength Dispersive X Ray Fluorescence (WDXRF) where energies split through the use of a crystal according to Bragg's Law. This allows for peaks with higher resolution in the spectrum at the expense of much longer acquisition times, for each energy has to be measured individually. Additionally, the setup is more complicated, more expensive and not as portable as the EDXRF setup.

A comparison between both setups is made in Figure 1.3.

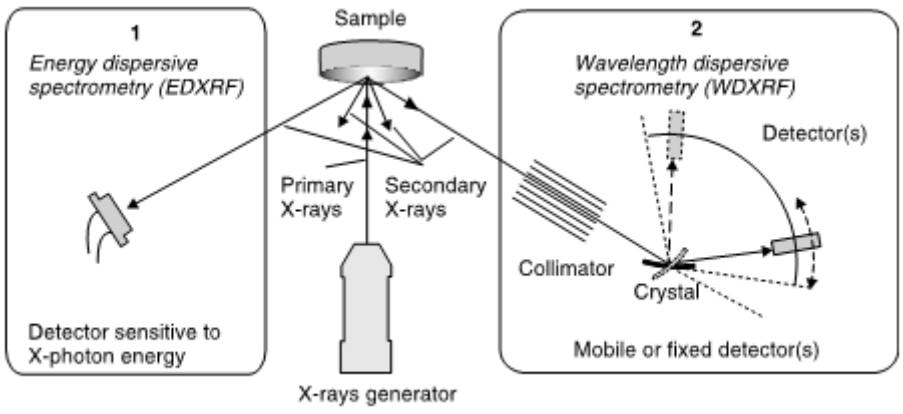

Figure 1.3: Comparison between EDXRF and WDXRF setups [14].

Two relevant variations of EDXRF are Total Reflection X Ray Fluorescence (TXRF) and micro X Energy Dispersive Ray Fluorescence (μEDXRF).

In TXRF the angle between the X Ray Tube and the sample is very close to the total reflection angle. This ensures that only the photons originated from fluorescence

phenomena, allowing for lower detection limits. Only thin samples can be used in this technique.

μEDXRF is similar to the classical EDXRF except that the X Ray beams are narrowed through the use of a polycapillary lens and focused to a much smaller area, allowing for much better spatial resolution, ranging from the millimetres to the tens of millimetres. This technique allows not only for the acquisition of different spectra for different regions of a sample, but also for the 2D mapping of each detected element across the sample. A setup of this kind will be used in this work.

1.3.5 Quantitative Analysis Using X Ray Fluorescence

X Ray Fluorescence techniques are a very powerful tool when it comes to identifying the elements present in the sample, but determining the exact concentration of those elements can be challenging due to matrix effects. In the absence of matrix effects, the intensity of the peaks in a spectrum would be proportional to the concentration of the elements correspondent to those peaks, but with the exception of very thin samples, matrix effects are unavoidable. These effects are the attenuation or enhancement of the fluorescence photons, due to their interactions with the matrix elements, affecting the intensity of the peaks in the XRF spectrum.

Figure 1.4, taken from R. Sitko and B. Zawisza's "Quantification in x-ray fluorescence spectrometry" [15], shows how the relative intensity of the peaks in a XRF spectrum corresponding to an element (in this case Fe) can be affected depending on the other elements present in the sample.

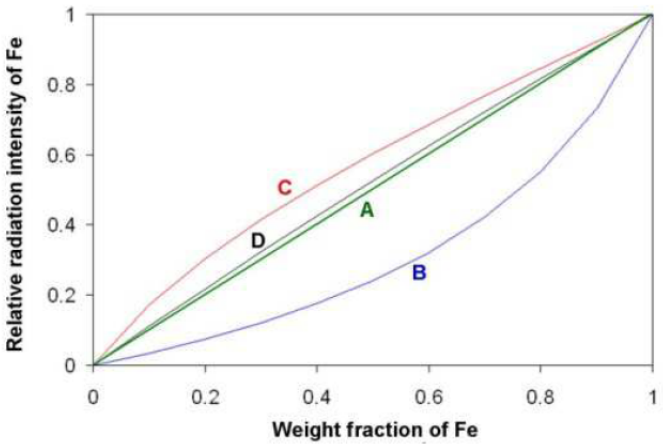

Figure 1.4: Relationship between radiation intensity of Fe and weight fraction of Fe: Curve A – matrix effects are negligible, Curve B – FeCr, Curve C – FeNi, Curve D – FeMn [15].

In curve B, the Fe fluorescence photons (6.4 keV)[16] have enough energy to remove electrons from the Cr atoms' K shell (binding energy = 6.0 keV)[16] and generate secondary fluorescence photons. This means that more Cr fluorescence photons and fewer

Fe fluorescence photons will reach the detector. In this situation, the intensity of the peaks will be misleading because it will suggest that there is less Fe in the sample than there actually is. The opposite happens in curve C, since the Ni fluorescence photons (7.4 keV)[16] have enough energy to remove electrons from the Fe atoms' K shell (binding energy = 7.1 keV)[16], which means that more Fe photons and fewer Ni photons will be detected. In this case, the intensity of the peaks would suggest that there is more Fe in the sample than there actually is.

The example in Figure 1.4 only considers the interactions between pairs of elements. In samples with more elements, the manifestation of the matrix effects can be more complex.

For thin samples, these effects are negligible, and therefore the intensity of the peaks is linearly proportional to the concentration of these elements. In these cases, the most appropriate method is the Internal Standard Method, which consists in adding to the sample a known quantity of an element not present in the sample. The intensity of the peak correspondent to that element will serve as a standard to quantify the other elements in the sample.

As sample thickness increases, linearity is lost and matrix elements must be taken into consideration.

A commonly used method to overcome this problem is the External Standard approach, which involves the comparison with Certified Reference Materials (CRM) in order to build calibration curves for each element [17]. This method has as its major drawback the need for a large number of CRMs for the obtained curves to be reliable.

On the other hand, there are methods, such as the Fundamental Parameter Method, that do not require the use of standards to quantify elements in a sample. This method iteratively compares theoretical intensities with the measured ones and estimates the composition of the sample when a suitable match is made [15]. However, it can be difficult to use this method when the matrix of the sample is composed of elements not visible in the XRF spectrum, such as H, C, N and O, but have a big influence on how trace elements are detected [18]. This is the case for human tissue. In order to obtain good results in these circumstances, a CRM of similar composition to the unknown sample can be used for calibration with this method [19, 20].

1.4 State of the Art

In this section is presented the result of the bibliography research. It contains the summarized findings of other researchers who approached similar themes and shown the suitability of X Ray Fluorescence techniques for analysing biological tissue, as well as interesting findings regarding the use of trace elements as biomarkers for carcinogenesis in various types of human tissue.

1.4.1 Quantification of Trace Elements in Human Tissues With X Ray Fluorescence

X Ray Fluorescence techniques have been widely used for the detection of elements in a sample, and the determination of their respective concentrations. For the detection of trace elements in human tissue, the most commonly used XRF techniques are TXRF and EDXRF. Magalhães et al. performed a study comparing the performance of TXRF and EDXRF for this purpose [21] and found that the results produced by both techniques are in agreement with each other. Furthermore, he considered both techniques to be complementary, TXRF being more sensitive to lighter elements and EDXRF slightly better in the detection of heavier elements.

The quantification method used in TXRF is generally the Internal Standard method, due to the minimal influence of matrix effects [22–25]. In the case of EDXRF, the chosen method is usually the External Standard method, with or without some form of intensity correction using the scattered radiation peaks [26–28].

In a study by Pessanha et al. [17] several methods of quantification for EDXRF were compared, and for the purpose of quantifying trace elements, similarly accurate results were obtained using the Fundamental Parameters method and the External Standard comparison method with intensity correction using Compton Scatter peaks. Both these methods being equally accurate for this purpose, the use of the Fundamental Parameters approach becomes advantageous due to the fact that it is not dependant on CRMs.

1.4.2 The Role of Trace Elements in Carcinogenesis

Many studies have found strong connections between imbalances in the concentration of trace elements and the formation of tumors. However, the variation of the concentration of these elements is not the same for all types of tumors. The concentration of these elements has been shown to vary differently depending on which tissue the tumor has formed from, as well as the tumor's degree of malignancy.

Regarding breast cancer, studies show a general tendency for the concentration of K, Fe, Cu, Zn and Br, to increase in tumorous tissue, when compared to normal tissue [24, 29]. Machado et al. [12] additionally found an increased concentration of P and S in cancer tissue than in normal tissue. They also found an increased concentration of K, but found no difference in the concentration of Zn between normal and cancer tissue. The degree of malignancy of these tumors seem to be associated with correlated concentrations of Fe and Cu, and Ca and Zn [27], and higher concentrations of Fe [22].

For tumors in uterus tissue, there seems to be an increase in the concentration of K and a decrease in the concentrations of Ca, Sr and Br, when compared to normal uterus tissue [21]. Machado et al. [12] also found differences in lighter elements such as an increase in the concentration P and S in cancer tissue comparatively to normal uterus tissue.

In brain tumors, Wandzilak et al. [30] have found an increase in the concentration of Zn, and a decrease in the concentration of Fe, P, S and Ca. They also found that the degree of malignancy of these tumors is related to a decrease in the average concentration of Fe.

Banas et al. [31] have linked prostate tumor formation with the excess concentrations of Mn, Fe, Cu, and Zn. However, the results shown by Carvalho et al. [29] seem to suggest that the increase or decrease in the concentration of Fe depends on the malignancy of the tumor. Additionally, a relevant increase in the concentration of K is also shown. Ensina et al. [18] have found results in agreement with Banas et al. [31] in terms of the behaviour of Fe and Cu and Zn, and have also shown an increase in S and Ca.

The study done by Ensina et al. [18] also shows a decrease of S, Ca, Fe, Cu and Zn in ovary tumor tissue relative to normal ovary tissue. These results are in agreement with the ones shown on Carvalho et al. [32] regarding Fe, Cu and Zn. Carvalho et al. have additionally shown a decrease in Br concentration in tumor tissue.

As for lung tumors, both Kubala-Kukus et al. [33] and Majewska et al. [25] found a decrease in the concentrations of Fe, Zn and Cu when compared to healthy tissues. Results found by Carvalho et al. [32] are compliant with the findings regarding Zn and Fe but contrary on those regarding Cu.

When it comes to colon tissue, Carvalho et al. [32] found a decrease in Fe, Cu, Br and Zn in tumor samples relative to the normal ones. However, Magalhães et al. [24] show increased concentrations of P, S, K, Cu, Zn and Rb, and decreased concentrations of Se and Br.

The existence of contradictory results for some cases heightens the importance of having a large number of samples in these studies, so that stronger conclusions may be drawn.

2

Materials and Methods

This chapter contains a description of the samples, equipment and software used in this work, as well as an explanation of the methodology used to develop the quantification method.

2.1 Samples

The samples used in this work can be divided into two groups, based on the purpose with which they were analyzed.

The **Reference Samples** were used to validate the quantification method, while the **Unknown Samples** were analyzed with the developed quantification method in order to compare the concentration of trace elements in normal and tumor tissue.

2.1.1 Reference Samples

The reference samples consisted of two groups of mirror samples.

The first set was obtained from donors at NOVA Medical School (NMS). Samples were collected from deceased patients donated through the Corpses Donation Office at the Department of Anatomy of NOVA Medical School for research and educational purposes. The subjects were embalmed using exclusively intra-arterial perfusion of a solution composed of aliphatic alcohols (diethylene glycol and monoethylene glycol), and then were kept in refrigerated cameras at 4 °C, with no further exposition to other fixatives or preservative alcohols, to ensure tissue preservation over time. Portions of bladder, colon, heart, intestine, liver, lung, muscle, stomach and uterus tissue were extracted, and each portion divided into two groups: one to be analyzed with Inductively Coupled Plasma Optical Emission Spectrometry ICP-OES, and another to be processed into Formalin Fixed Paraffin Embedded (FFPE) samples. The whole sample preparation and analysis process is summarized in figure 2.1.

The second set was extracted at Instituto Português de Oncologia (IPOLFG). Similarly, portions of breast and colon tissue were extracted and divided to create lyophilized samples and the other to create Formalin Fixed Paraffin Embedded (FFPE) samples.

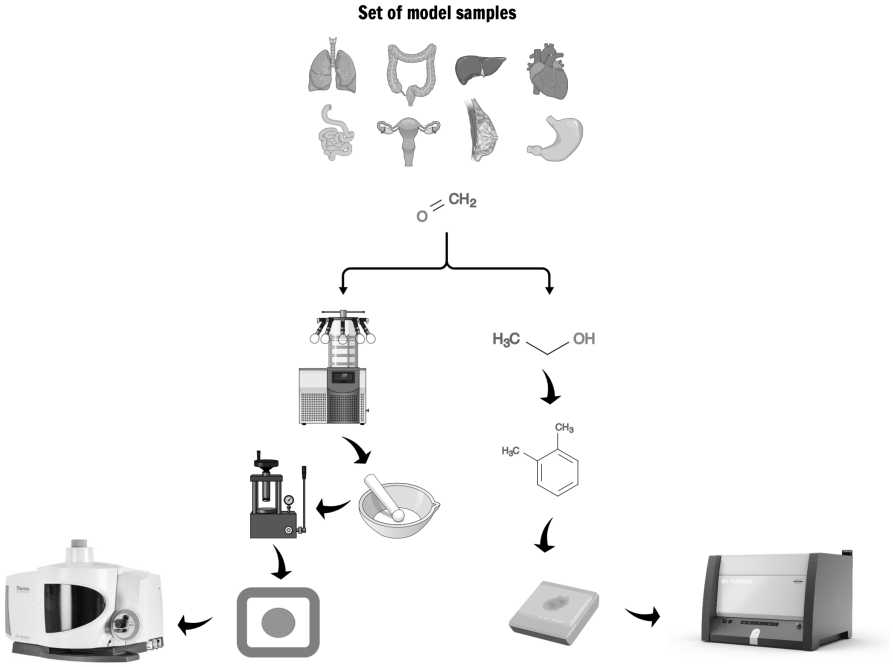

Figure 2.1: Sample preparation workflows for ICP-OES analysis (left branch) and μEDXRF (right branch).

2.1.2 Unknown Samples

These samples were kindly provided by the Pathologic Anatomy unit of the Centro Hospitalar Barreiro Montijo. The samples consist of surgically removed tissue from individuals diagnosed with breast or colon tumors, fixed in formalin and embedded in paraffin for preservation. All samples were duly anonymized.

These Formalin Fixed Paraffin Embedded (FFPE) samples were grouped into pairs of normal and tumor tissue from each individual. A total of 30 colon pairs and 28 breast pairs of samples were analyzed without the need for any sort of added preparation.

2.2 The R Project for Statistical Computing

Figure 2.2: R Logo [34].

From the early stages of planning this work, it was clear that there would be the need for a programming tool to analyze the mappings of the various elements.

R is a free programming language best suited for statistical data analysis and graphics [35]. One of R's main advantages is its easy extensibility through the use of packages, which broadens its potential applications beyond just the field of statistics. In this work, two packages were of extreme importance: countcolors and colordistance. By combining these two libraries, it is possible to select areas of

images based on their color or intensity, which was crucial in finding the best regions of sample to analyze.

The statistical treatment of the data obtained in this work was also done in R.

2.3 Mapping the Samples

Samples were analyzed using Bruker's M4 Tornado XRF Spectrometer. The X-Ray tube was set at a voltage of 50 kV and a current of 300 μA for all measurements. The chosen size for each pixel was 25 μm and the air pressure inside the chamber was set as 20 mbar.

Figure 2.3: Bruker's M4 Tornado μXRF Spectrometer [36].

The system was used considering two different filter configurations: using a 12.5 μm Al filter for the removal of the contribution of the Rh-L scattering peaks and improvement of detection limits for lighter elements (Z<20) and using a combination of filters 100 μm Al, 50 μm Ti and 25 μm Cu for background reduction and improvement of detection limits for heavier elements (Z≥20).

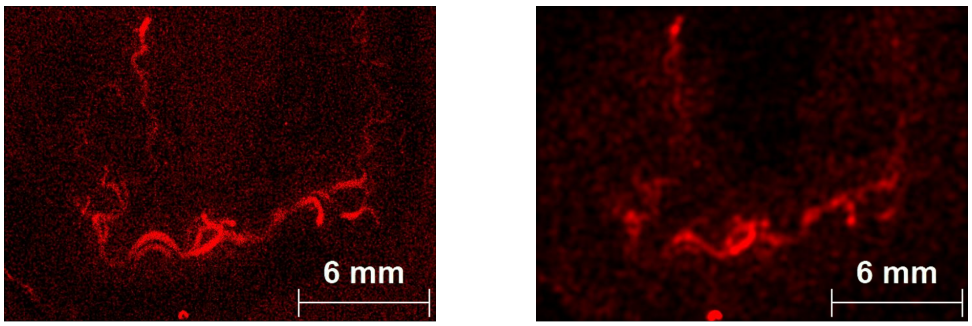

(a) Al 12.5 μm filter (b) Al/Ti/Cu 100/50/25 μm filter

Figure 2.4: Fe mappings of a colon sample.

Each sample was scanned twice, once with each of the filter configurations. The majority of the area of all samples was scanned. The average scan duration was 2 hours and 30 minutes.

2.4 Locating Tissue in Paraffin

The paraffin poses an obstacle in quantification, for it consists of mainly hydrogen and carbon, elements that are invisible through XRF, but have a significant impact on the characterization of the matrix. Besides, the FFPE samples have regions containing only paraffin, and in some cases, it is not easy to tell them apart from those that actually contain the tissue.

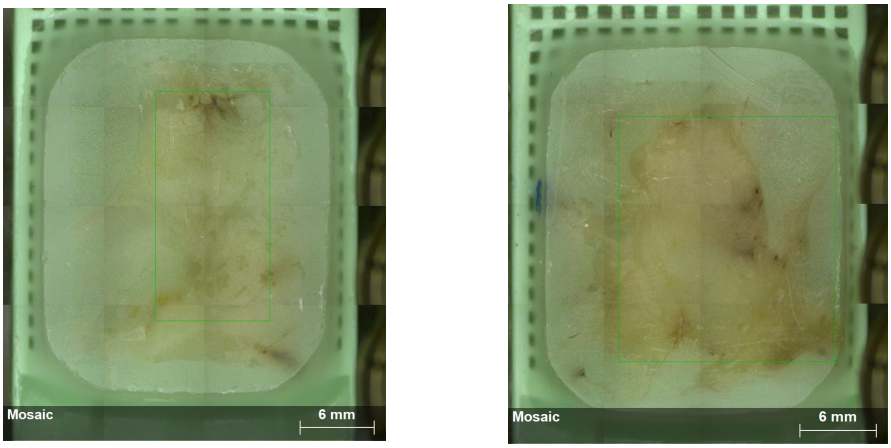

Figure 2.5: Breast FFPE Samples.

In an attempt to minimize the paraffin's influence in the quantification results, an algorithm was developed to determine which areas of the sample were more suited for analysis and quantification. The areas sought were those that had thinner layers of paraffin covering and embedding the sample. To find these areas, two approaches were devised:

- **Approach A**, which targets broad areas of tissue and has as its main goal excluding regions containing only paraffin or a relatively thicker layer of paraffin over the tissue;
- **Approach B**, which took approach A a step further in terms of specificity and targeted the tissue containing areas with thinner layers of paraffin covering the sample, while also excluding regions of haemorrhaging and calcification;

2.4.1 Approach A

The first approach focused mainly on the mappings of sulphur. The main reason for choosing this element was its low emission energy (S Kα = 2.3 keV), which is highly attenuated by the paraffin. This means that the areas with higher intensity in the sulphur mappings correspond to those with thinner paraffin layers covering the sample, and for that reason, are also the areas more suited to be quantified. Moreover, this element presents other advantages:

- It is one of the most abundant elements in human tissue samples, so its detection is simple;
- It is relatively homogeneous in the tissue, meaning that there is no evidence of S clustering;
- It is not present in the paraffin, conversely to Ni, Cu and Zn as determined in previous studies;

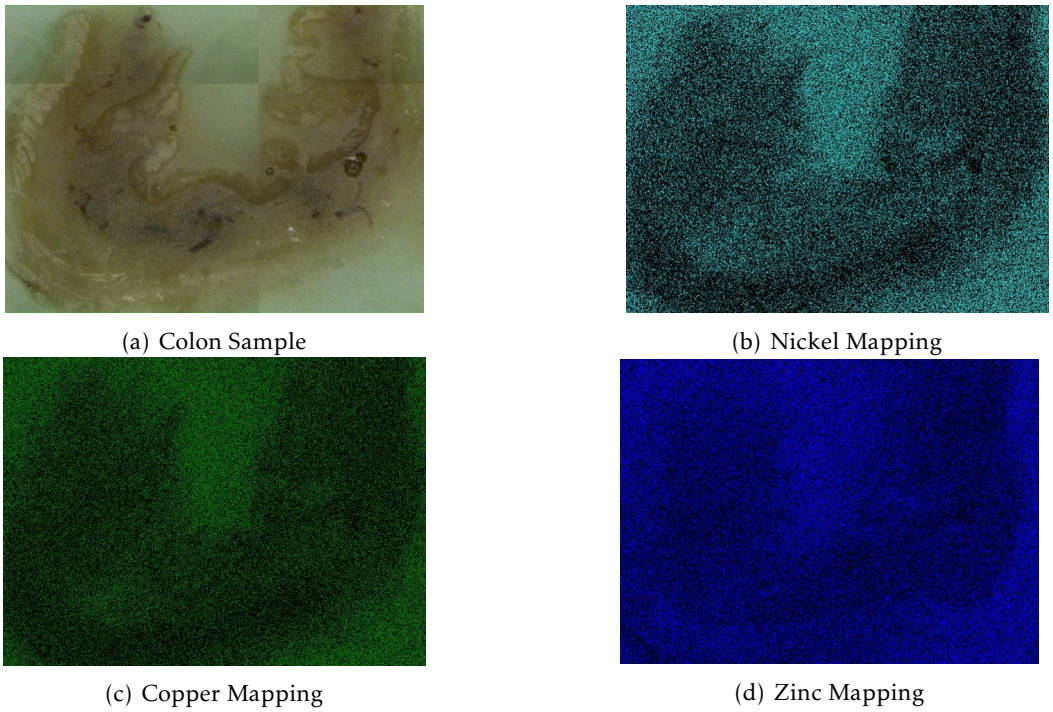

(a) Colon Sample (b) Nickel Mapping

(c) Copper Mapping (d) Zinc Mapping

Figure 2.6: Nickel, copper and zinc mappings of a colon sample.

By looking at figure 2.6, it is clear that Ni, Cu and Zn show higher intensity in areas containing no tissue, which shows the presence of copper and zinc in the paraffin.

The algorithm for approach A is represented in figure 2.7:

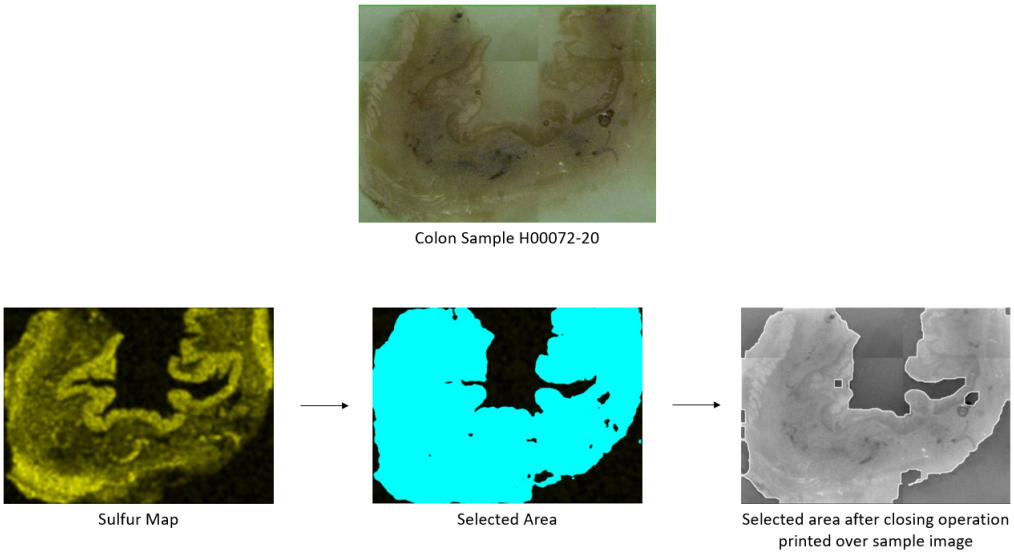

Figure 2.7: Area selection through Approach A.

The way the selected area depicted in figure 2.7 was found was through the combined use of two R libraries: R©Colordistance and R©Countcolors. By combining these two libraries, it is possible to select areas of images based on their colour or intensity. Using the R©Colordistance, a subset of 10000 randomly selected pixels from the S mapping image was selected in order to speed up the computing process. Each of those pixels was treated as a point in a three dimensional space according to their RGB values, as represented in figure 2.8.

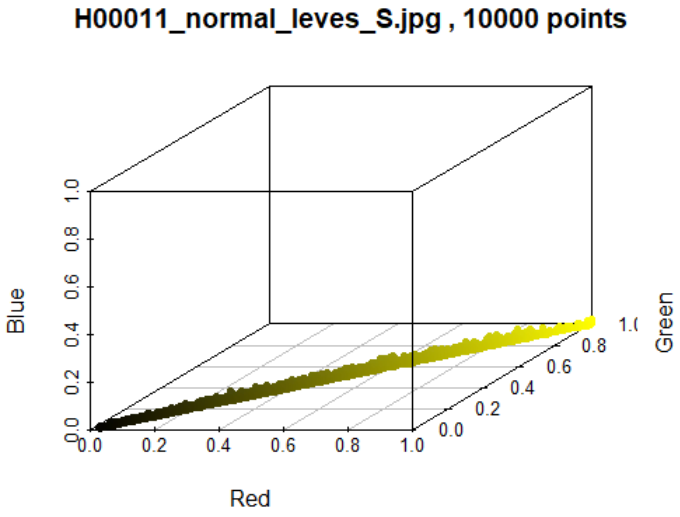

Figure 2.8: Representation of a subset of 10000 pixels from a sulphur mapping on a 3-dimensional RGB space.

Through the use of a k-means algorithm, the pixels were split into three different clusters, and the mean RGB values of each of them were stored. An example of the resulting clusters on a sulphur mapping is represented in figure 2.9.

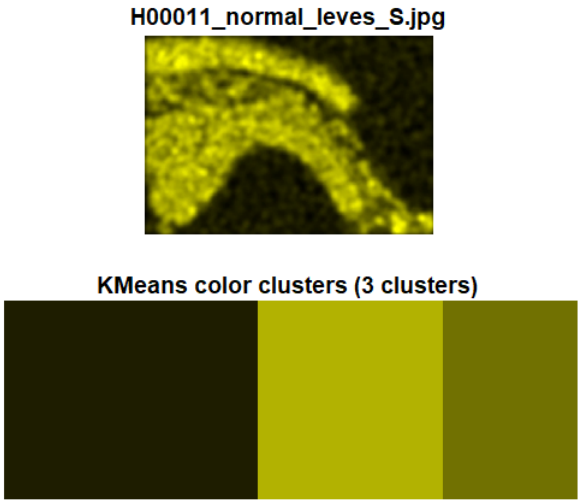

Figure 2.9: Representation of the extracted clusters through the kmeans algorithm.

Then, by using the R©Countcolors, all pixels with higher intensity (higher RGB values) than the mean of the second most intense cluster were selected. To eliminate small holes in the selected area, a closing operation was performed (dilation followed by an erosion). A square mask with a size of 15 pixels was used. The selected area was then plotted over a grayscale picture of the sample, as depicted in the final step of figure 2.7.

2.4.2 Approach B

This second approach also tracks the intensity of sulphur in the mapped areas, but it also focuses on other elements:

- Phosphorus – similarly to S, it is an element with low emission energy (P Kα = 2.0 keV), and could be used as confirmation;
- Calcium - areas presenting high concentration of this element should be avoided because they might be due to calcifications;
- Iron – present in blood so areas presenting high intensity of this element might be indicative of haemorrhaging, which should be avoided;

The selected areas are those with high intensity in both sulphur and phosphorus mappings, and if in those selected areas there are regions with peak intensities of either calcium or iron, those are excluded. The algorithm for approach B is represented in figure 2.10:

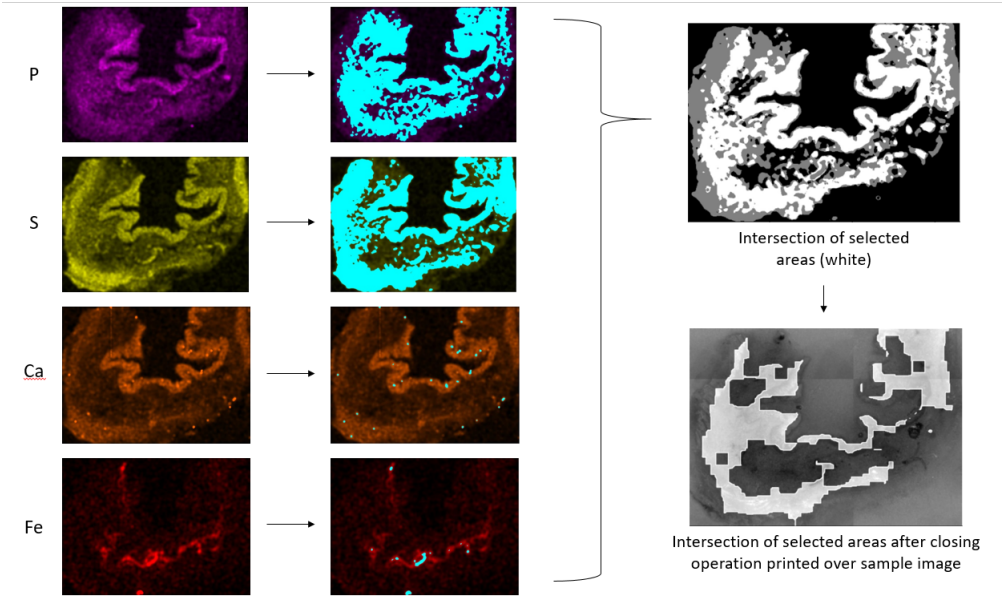

Figure 2.10: Area selection through Approach B.

In Approach B, the treatment of the Sulphur and Phosphorus mappings was similar to the one done in Approach A, except that the pixels were split into four clusters rather than three. Again, all the pixels with higher intensity than the mean of the second most intense cluster were marked.

As for the calcium and iron mappings, thresholds were defined since not all samples had peaks of these elements, and marking the most intense pixels could result in the exclusion of areas suited for analysis in those cases. The chosen RGB values were (0.8, 0.2, 0) for calcium, which had orange mappings, and (0.8, 0, 0) for iron, which had red mappings. These areas are represented graphically in figures 2.11 and 2.12 respectively.

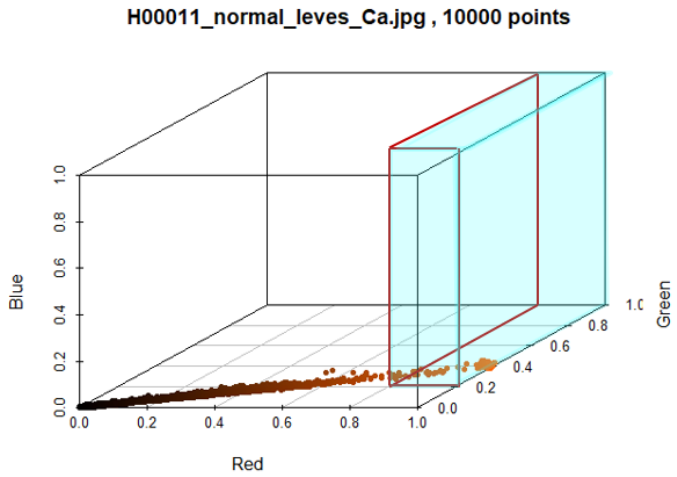

Figure 2.11: Selected regions of the RGB 3-dimensional space for calcium mappings

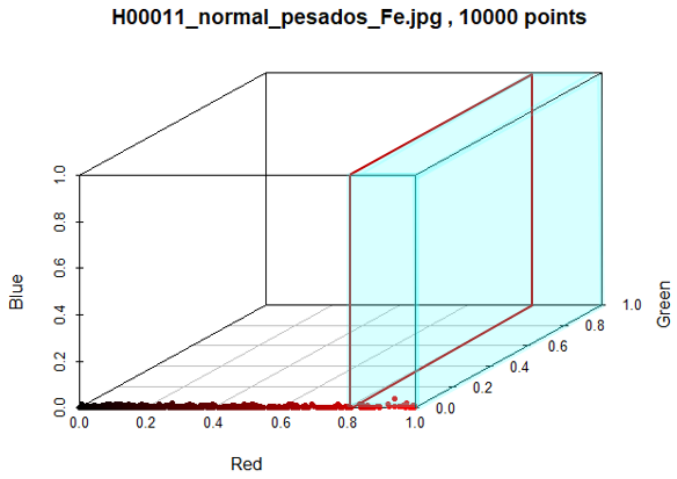

Figure 2.12: Selected regions of the RGB 3-dimensional space for iron mappings.

2.5 Dark Matrix Determination

As mentioned previously, the main obstacle in the development of a standardless quantification method for samples of human tissue preserved in paraffin is the fact that the most abundant elements in the samples (H, C, N and O) are invisible to the XRF analysis – dark matrix - but greatly influence the quantification of elements such as P, S and K due to matrix effects.

The M4 Tornado software has a built-in fundamental parameters quantification code, but it requires a matrix composition to be given as input. This code has been used successfully in the quantification of bone [37] and metal samples [38], where either the matrix was known or all the elements were visible in the EDXRF spectrum.

In order to build a quantification method capable of overcoming the difficulties imposed by the paraffin, taking advantage of the M4 Tornado software's fundamental parameters quantification code, the first step was determining the composition of the matrix of the samples. This section contains the various attempts, and all the steps taken to accomplish that task.

2.5.1 Mirror Samples analyzed With ICP-OES

The impact that the the paraffin would have on the quantification results was uncertain, and for that reason, it was important to have the same tissues analyzed with a highly reliable technique in order to compare results and validate the Dark Matrix Composition.

Prior to this work, portions of tissue from several organs of the same donor were extracted at the Department of Anatomy of NOVA Medical School and divided into groups in order to be analyzed and quantified through different methods, as mentioned in section

2.1. The results obtained from the analysis of those tissues with ICP-OES are shown on table 2.1.

Table 2.1: ICP-OES Results (in μg/g).

	P	S	K	Ca	Cu	Fe	Zn
Liver	1940 ± 60	10000 ± 300	3010 ± 70	1180 ± 40	9.95 ± 0.04	98 ± 2	75.5 ± 0.5
Uter	1370 ± 40	9500 ± 100	1805 ± 5	430 ± 6	2.38 ± 0.02	60 ± 1	39 ± 1
Colon	1500 ± 400	8000 ± 1000	3400 ± 500	980 ± 80	2.8 ± 0.4	69 ± 9	55 ± 9
Heart	2200 ± 300	12000 ± 1000	3200 ± 400	520 ± 60	3.8 ± 0.4	90 ± 9	110 ± 20
Intestine	940 ± 60	9800 ± 200	1500 ± 100	800 ± 100	5.3 ± 0.6	130 ± 20	117 ± 9
Stomach	1640 ± 40	10400 ± 500	1900 ± 100	260 ± 20	3.6 ± 0.2	81 ± 4	53 ± 1
Muscle	1300 ± 50	16900 ± 800	1380 ± 80	1000 ± 100	2.82 ± 0.01	124 ± 4	221 ± 5
Skin	800 ± 20	2800 ± 200	450 ± 20	200 ± 10	0.72 ± 0.05	27.7 ± 0.3	44 ± 2
Bladder	1600 ± 70	9900 ± 300	1750 ± 80	2080 ± 80	4.6 ± 0.3	150 ± 30	65 ± 5
Lung	1760 ± 30	10200 ± 200	1730 ± 30	360 ± 20	2.4 ± 0.1	183 ± 3	47 ± 1

Additionally, to test the accuracy of this technique, an oyster CRM was analyzed, and produced the results shown on table 2.2.

Table 2.2: ICP-OES Results for the Oyster CRM (in μg/g).

		S	K	Ca	Fe	Cu	Zn
CRM Oyster	**Reference**	6900 ± 200	6520 ± 90	840 ± 20	206 ± 7	72 ± 2	1420 ± 50
	ICP-OES	7400 ± 80	6600 ± 100	756 ± 6	210 ± 6	78 ± 2	1600 ± 30

Due to the high accuracy of this technique, shown by the proximity between the obtained results and the reference values for the oyster CRM, the results of the ICP-OES quantification were used as the reference values for the validation of the Dark Matrix composition.

The fact that one of the sets of reference values was obtained with colon tissue is an advantage, since one of the tissues studied in this work will be colon. Unfortunately, none of the sets of values was obtained from breast tissue, but having a variety of other tissues can help validate the method for breast tissue if the quantification with the chosen Dark Matrix is shown to be effective for all tissues.

Having established the reference values, the next step was determining a matrix composition that, when inserted in the M4 Tornado software, would produce quantification results that match those reference values.

The first attempted sets of values for H, C, N and O were conceived based on the premise that the matrix should consist of a certain percentage of human tissue, and the remaining percentage would be paraffin. The values for an average human tissue composition were inspired in many of the ICRU compounds available on the NIST website [39], as well as in the values stated in Glover's Pocket Ref [40] and *DarkM* from Ensina et al. [18]. The following values were chosen as an average elemental composition of the human body: 10% H; 19% C; 3% N and 65% O. As for the paraffin, it was assumed that it would be mainly composed of compounds described by the formula C_nH_{2n+2}, and would thus have a composition of approximately 67% H and 33% C. Given these assumptions,

eight different potential compositions for the dark matrix were calculated by changing the ratio between human tissue and paraffin. The compositions of these 8 matrices are presented on table 2.3.

Table 2.3: Compositions of the potential dark matrices.

Matrix	**1**	**2**	**3**	**4**	**5**	**6**	**7**	**8**
% of H	13	15	18	21	24	26	29	32
% of C	19	20	21	21	22	23	24	24
% of N	3	3	3	3	2	2	2	2
% of O	62	59	55	52	49	46	42	39
fraction of tissue	0.95	0.90	0.85	0.80	0.75	0.70	0.65	0.60
fraction of paraffin	0.05	0.10	0.15	0.20	0.25	0.30	0.35	0.40

These eight compositions were used to quantify the FFPE samples with the M4 Tornado Software. All the samples were mapped in the M4 Tornado spectrometer with both filters and the areas were selected using Approach A described in section 2.7. The light elements (P, S and K) were quantified in the spectrum obtained with the 12.5 μm Al filter, and the remaining heavy elements were quantified in the spectrum obtained with the Al/Ti/Cu 100/50/25 μm filter.

The deviation from the reference values for each tissue is shown in figure 2.13 for the colon sample, and figure 2.14 for four of the remaining eight tissues. The graphs of all remaining eight tissues are available in Annex I. It is important to note that the chart's y axis is limited to 100, to facilitate analysis. In the case of Cu for many of the tissues, the deviation vastly exceeded 100%, which can be explained by it's low concentration in the tissue, as shown on table 2.1, and it's presence in the paraffin.

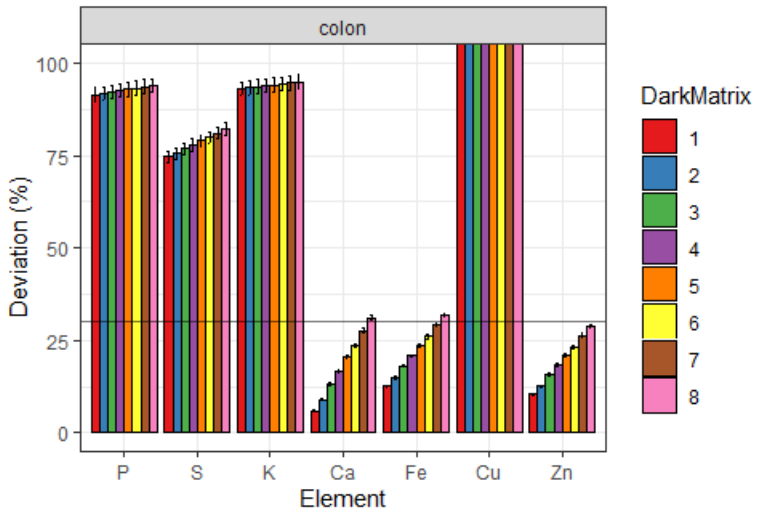

Figure 2.13: Deviation of the quantification results of the FFPE colon sample from reference value (in %).

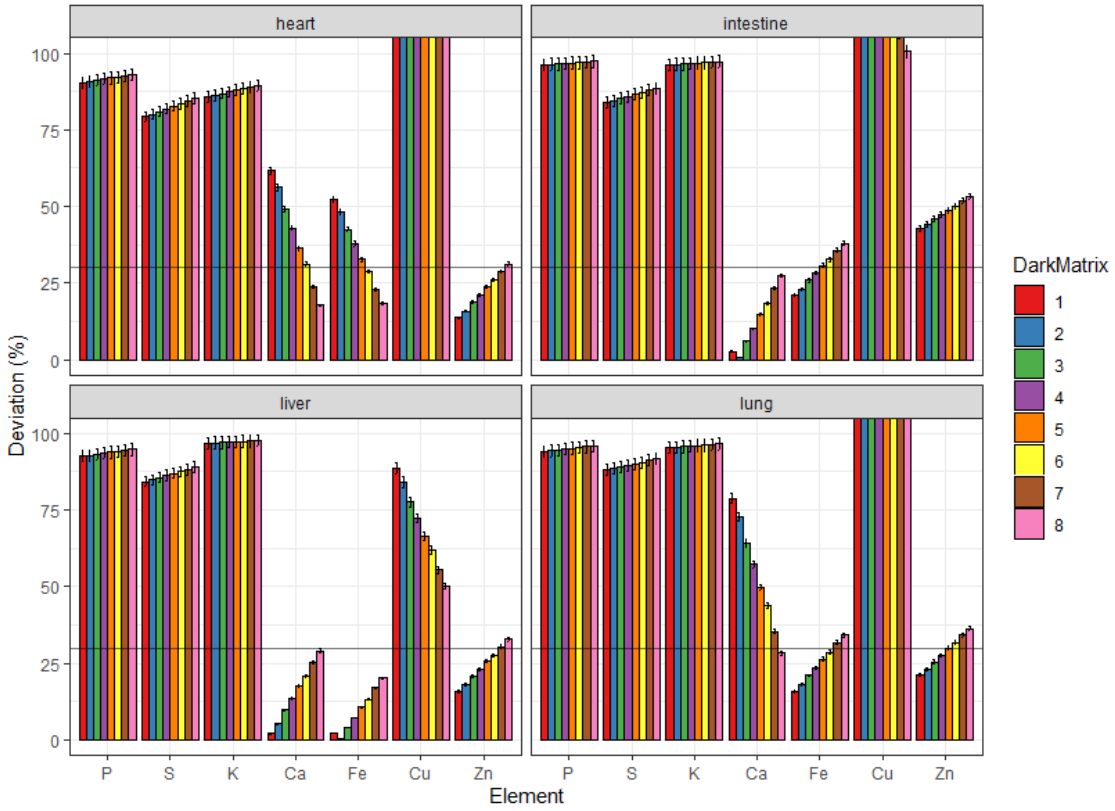

Figure 2.14: Deviation of the quantification results of the FFPE heart, intestine, liver and lung samples from reference values (in %).

Some conclusions can be drawn from figures 2.13 and 2.14:

- The elements with Z < 20 (P, S and K) show deviations above 75% regardless of tissue and composition of Dark Matrix. This indicates that the influence of paraffin in the detection of these elements much higher than initially expected.

- Despite the high deviation on the elements with Z < 20 and copper (due to its presence in the paraffin and its low amount in the paraffin), for almost all the tissues analyzed, there is at least one of the eight Dark Matrices that produces deviations under 30% for Ca, Fe and Zn, which suggests that this method might be suitable for quantifying heavy elements.

- Dark Matrices 1 through 8 show better results depending on the tissue. Looking at the colon graph in figure 2.13, it is clear that DarkMatrix 1 shows less deviation than the others, and is therefore likely to be the best suited for this tissue. In figure 2.14, the intestine and liver charts also seem to suggest that the best suited matrix is DarkMatrix 1. However, in the cases of heart and lung, for example, DarkMatrices 6, 7 and 8 seem to have the least overall deviation for for Ca, Fe and Zn. Assuming

that the ratio of human tissue to paraffin is similar across all the samples, this may suggest a need for different matrices for different kinds of tissues.

Unfortunately, this approach had to be disregarded. In another work being developed in parallel to this one by Alexandre Veiga and his advisors, it was discovered that the time that the tissue spends in the formalin causes very significant changes in the concentration of the trace elements.

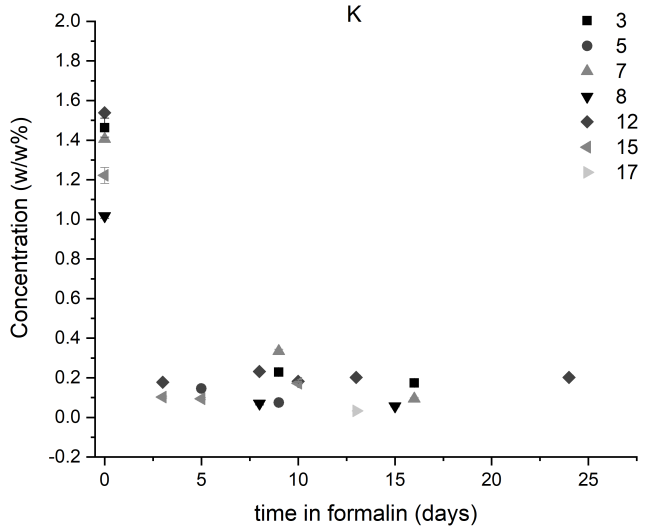

Figure 2.15: Evolution of the concentration of K in in tissue fixed in formalin over time.

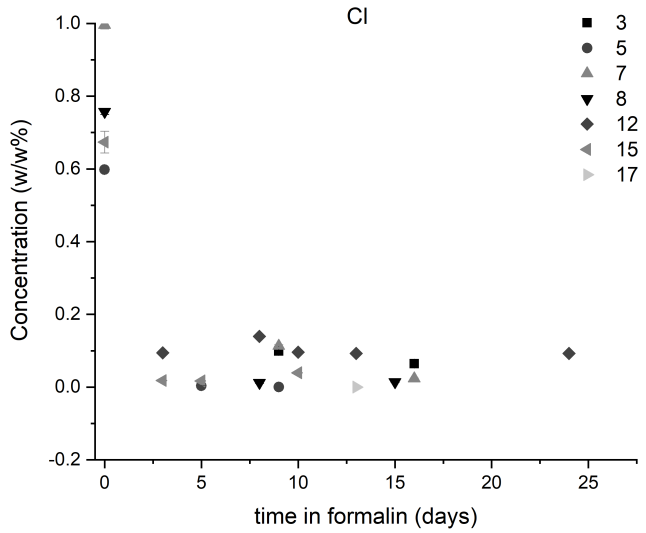

Figure 2.16: Evolution of the concentration of Cl in in tissue fixed in formalin over time.

Figures 2.15 and 2.16 present the decrease of concentration of K and Cl in tissue, with time in formalin. Quantification of the elements present in the samples was performed using the Fundamental Parameters Method, considering the DarkM matrix (0% H, 22% C, 3% N and 60% O.) [18]. As can be seen, after 3 days, K and Cl decreases over 70%.

The samples analyzed through ICP-OES were not fixed in formalin for the same amount of time as the FFPE ones. One portion of the samples was only preserved in formalin for a few hours until placed in the freeze-dryer for lyophilization, while the other portion underwent the common procedure for paraffin embedding that establishes a time for fixation in formalin ranging from 5-10 days. This way, the direct comparison between the two groups of samples is not valid, and so, there is no way to validate the choice of the Dark Matrix composition through this method.

The mechanisms that cause these changes are still unknown, and it would be interesting to study them in future works.

2.5.2 Mean Z approach

Taking into consideration the information learned through the previous approach, and the possibility of the need of different matrices for different tissues, the goal of this approach is to determine the composition of the Dark Matrix based on the mean Z of the samples.

It is known that the intensity of the scattered radiation depends on the Z of the sample. By analyzing the spectra of the colon and breast FFPE samples and determining their Compton-to-Rayleigh ratio, it is possible to determine the mean Z of the samples of each tissue, and build the Dark Matrix Composition according to the obtained value. The Compton-to-Rayleigh ratio can be calculated by dividing the amplitude of the Compton and Rayleigh peaks corespondent to the characteristic radiation from the X-Ray source of the spectrometer, in this case Rh. Those peaks are shown in figure 2.17, which contains a spectrum of one of the normal colon FFPE samples.

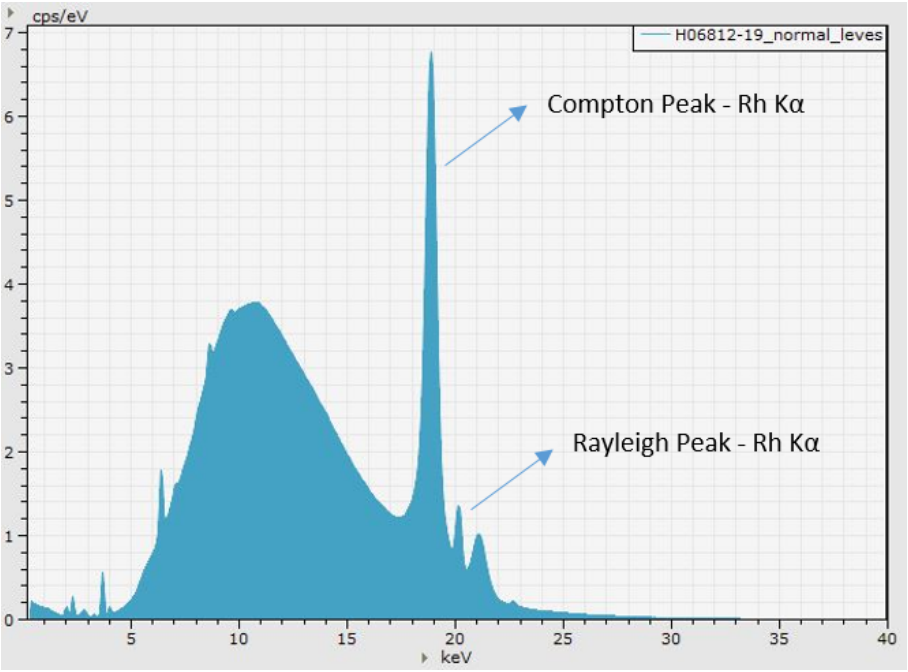

Figure 2.17: Rh Kα Compton and Rayleigh peaks.

In previous works, Pessanha et al.[11] developed and used a function establishing the dependency of the Compton-to-Rayleigh ratio of the scattering peaks of the X Ray tube with the mean Z of the scattering sample, for a given geometry and acquisition parameters. This curve was created using standard samples of hydroxyapatite and boric acid in variable concentrations, obtaining a range of mean Z samples from 7 to 14.

Using those same reference samples, the curve was built using the measurement conditions mentioned in section 2.3. In order to add points of lower Z to the curve, two extra samples were analyzed: a polymethyl methacrylate (PMMA) and a paraffin block. The resulting curve and respective function describing the Compton-to-Rayleigh ratio of the characteristic lines of the X Ray source of the spectrometer as a function of the sample's mean Z is shown in figure 2.18. Each point represents the average of 4 measurements, the uncertainty is the max deviation to the mean.

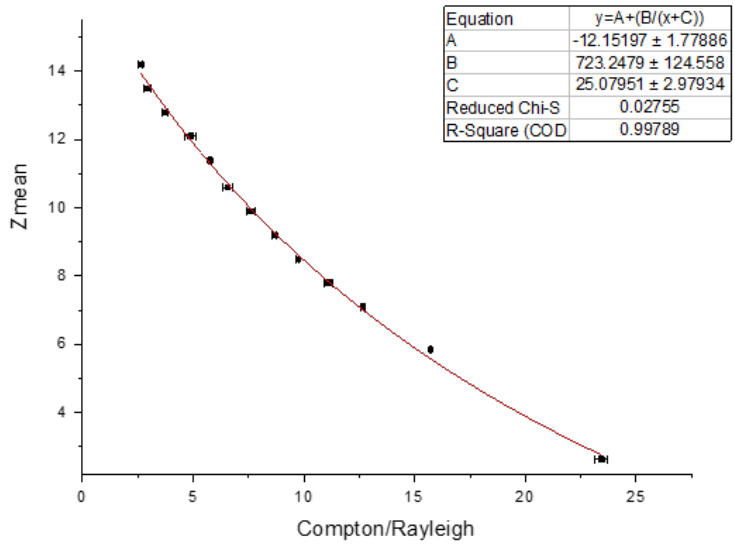

Figure 2.18: Sample mean Z as a function of the Compton-to-Rayleigh ratio.

In order to gauge the matrix average Z of the FFPE samples, the Compton-to-Rayleigh ratios of 3 samples from each tissue were determined. The mean Z was extrapolated to be 5.01 ± 0.09 for the colon samples, and 4.7 ± 0.2 for the breast samples. A graph showing both tissues fitted into the previously shown curve is presented on figure 2.19.

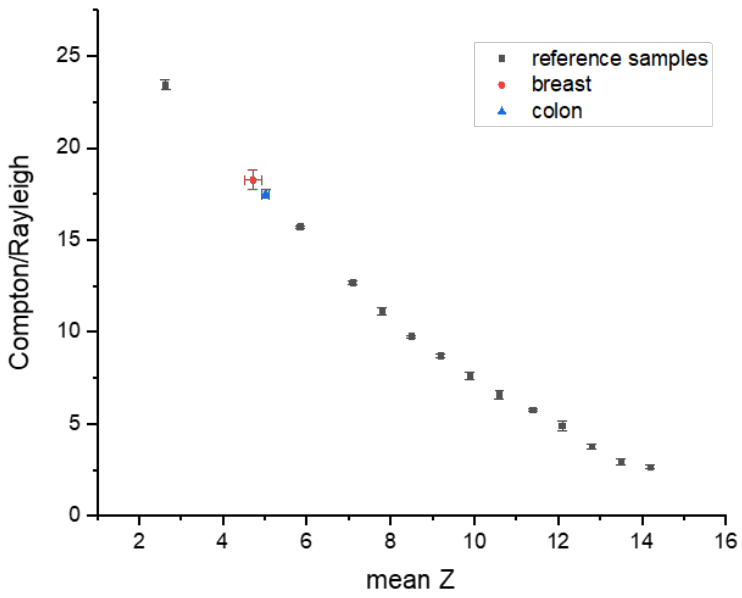

Figure 2.19: Compton-to-Rayleigh ratio as a function of sample Mean Z.

An interesting point that can be taken from figure 2.19 is the fact that the mean Z of the breast samples is smaller than the colon samples' mean Z, which was expected due to the fact that breast tissue has a higher percentage of carbon and a lower percentage of oxygen than all the ICRU-44 materials in the NIST website [39]. Since carbon has a Z=6 and oxygen has a Z=8, the measured mean Z of breast was expected to be lower.

It is also noticeable in figure 2.19 that the error bars in the point correspondent to breast are significantly larger that those of the point correspondent to colon. This higher uncertainty in the breast samples' mean Z might be due to some variability introduced by fat content.

In accordance to the information acquired regarding the samples' mean Z, a script was developed in R to compile multiple possible compositions of matrices, with H and C and ranging form 10 to 40%, N ranging from 1 to 3, and O ranging from 30 to 60%. Since the added percentage of the studied trace elements in this work wasn't expected to exceed 2%, the selection was narrowed down to compositions in which the sum of the percentages of H, C, N and O was equal to 98%. Out of the 2023 compiled compositions, those with a mean Z of 4.7 or 5 were selected. At this point, the selection consisted of 89 matrix compositions with a mean Z of 5 and 21 matrix compositions with a mean Z of 4.7. From the 89 with mean Z = 5, three representative compositions were selected. Those Dark Matrix compositions are presented on table 2.4. From the 21 with mean Z = 4.7, two representative compositions were selected. Those Dark Matrix compositions are presented on table 2.5.

Table 2.4: Colon Dark Matrix Compositions (in %).

	H	**C**	**N**	**O**
Dark Matrix 1	38	11	3	46
Dark Matrix 2	36	22	2	38
Dark Matrix 3	33	33	1	31

Table 2.5: Breast Dark Matrix Compositions (in %).

	H	**C**	**N**	**O**
Dark Matrix 4	39	22	2	35
Dark Matrix 5	38	28	1	31

The selection of these representative matrix compositions was based on the percentage of carbon. Within each group of matrix compositions, it was noted that, for the mean Z to be constant and for the sum of all percentages to remain equal to 98, the matrix compositions with a lower percentage of carbon had higher percentages of the remaining elements, and matrix compositions with a higher percentage of carbon had lower percentages of the remaining elements. Regarding these observations, the representative matrix compositions selected differed in the values of the percentage of carbon in a way that

would cover the range of values and infer whether the suitability of a matrix is due to its mean Z or the percentage of certain elements.

2.6 Quantification Method

In order to validate the used matrices, the second set of reference samples was analyzed with and without paraffin embedding. Portions of tissue were extracted at Instituto Português de Oncologia (IPOLFG). Those portions were then divided in two, one to go through the paraffin embedding process, while other was lyophilized and analyzed directly using EDXRF. The difference from the previous set of model samples was that these samples were fixated in formalin for, at least, three days. This way, the influence in formalin was diminished. Samples were labeled B, C1 and C2. Samples C1 and C2 were colon samples, while sample B was a breast sample.

These lyophilized samples were quantified considering DarkM as the matrix composition (10% H, 22% C, 3% N and 60% O) [18]. The quantification results are stated in tables 2.6 and 2.7.

Table 2.6: Lyophilized samples' quantification results in μg/g (Z < 20).

	P	S	Cl	K
B	7900±800	4900±400	140±20	1200±100
C1	7100±500	4500±600	1200±100	3500±300
C2	8100±500	3700±400	210±50	1100±200

Table 2.7: Lyophilized samples' quantification results in μg/g (Z ≥ 20).

	Ca	Fe	Ni	Cu	Zn
B	700±200	170±20	6.6±0.9	11.0±2.0	118±6
C1	1030±60	160±20	6.7±0.6	16.0±3.0	160±20
C2	780±80	320±60	6.0±2.0	11.0±3.0	160±50

The paraffin embedded samples correspondent to the lyophilized ones were then analyzed and quantified using each of the five Dark Matrix compositions. The deviations in percentages from the values in tables 2.6 and 2.7 are shown in figure 2.20.

Many of the analyzed elements show deviations well above the 30% threshold with either of the Dark Matrix compositions. Even considering the variability within the two portions of the mirrored samples, and that the formalin fixation could present a major factor of uncertainty, the obtained results cannot be considered satisfactory. All of the deviations presented in figure 2.20 are due to undervaluing, meaning that the paraffin imposes a big obstacle not only in the quantitative analysis, which was expected, but also in the detection of the X-Ray fluorescence photons. Cl and K were not included in the graphs of figure 2.20 because they showed values of 0% or very near 0%, even in sample C1, which has a concentrations over 1000 μg/g in the lyophilized mirror sample. Most

likely these elements are now under the detection limit of the method. For the purpose of this work, Cl and K will be excluded from analysis from this point onward.

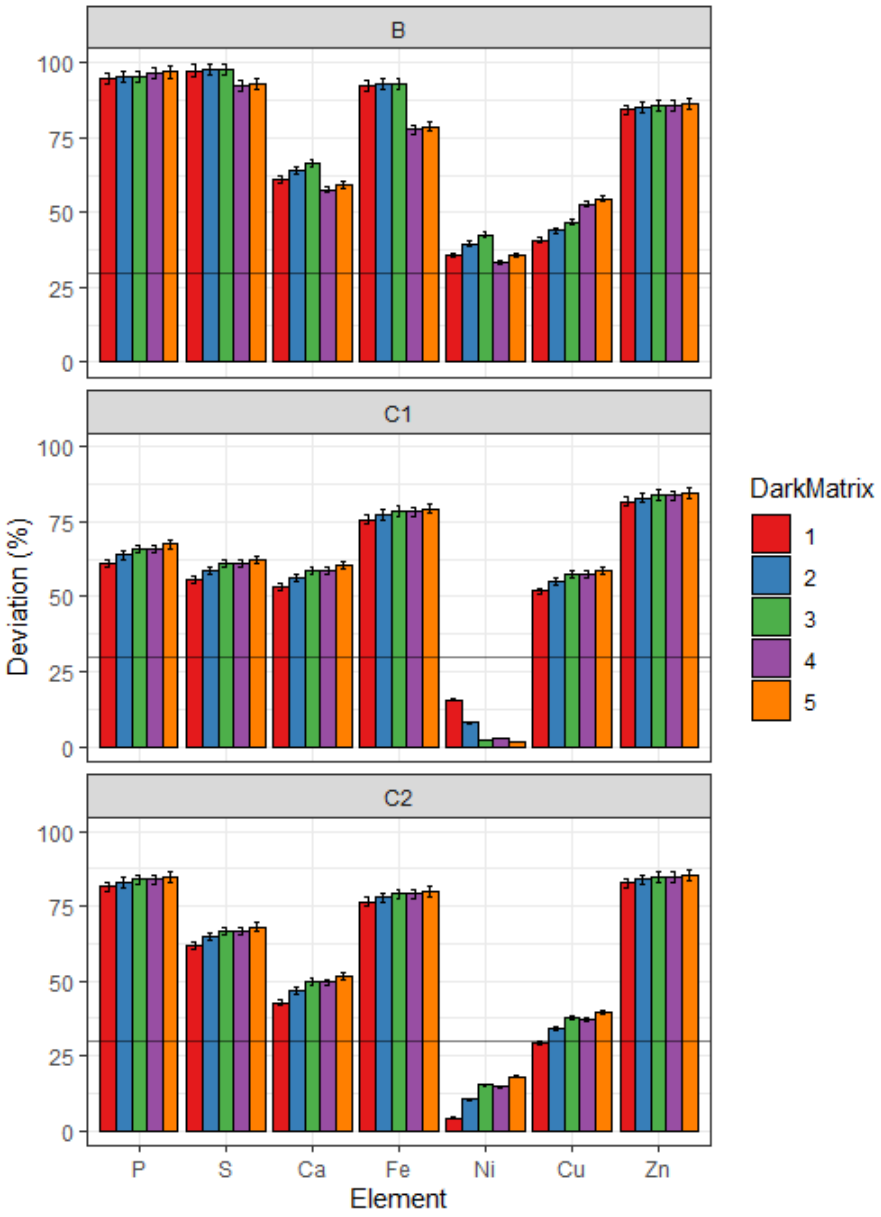

Figure 2.20: Deviations from reference values (in %).

Even though most elements show deviations above 30%, some conclusions about the suitability of these matrix compositions can be drawn. The percent deviations between the 5 matrix compositions tested do not differ largely. Still, the small differences displayed between them can be used to select the one that is slightly better suited to be used in quantifying FFPE samples. It is clear that for the colon samples (C1 and C2), Dark Matrix 1 shows the least deviation for all elements with the exception of Ni on sample 7, but since in that case the deviation is below 30%, Dark Matrix 1 can be considered the most

suited for colon FFPE samples. As for the breast sample (B), depending on the element Dark Matrix 1 or Dark Matrix 4 show the least deviation. Since Dark Matrix 4 shows the least deviation in four out of the seven analyzed elements (Ca, Fe, Ni, and S), it can be considered the most suited for breast FFPE samples.

By testing all five matrix compositions on all three samples, it was possible to test if the matrix compositions with a mean Z of 5 produced less deviation in colon, and if those with a mean Z of 4.7 produced less deviation in breast. The fact that Dark Matrix 1 (mean Z = 5) was shown to be the most suited for colon and Dark Matrix 4 (mean Z = 4.7) was shown to be the most suited for breast, that prediction was confirmed. Also worth mentioning is the fact that, among both groups of matrices (those with a mean Z of 5 and those with a mean Z of 4.7), the ones that showed less deviation from the reference values were those with higher percentages of N and O, and lower percentages of C.

A factor that should also be addressed regarding the undervaluing of the analyzed elements is the poor fit to the spectra.

As visible in figures 2.21 and 2.22, the peaks aren't properly fitted. This might be due to the poor signal to noise ratio, which is a consequence of the difficulties in detecting the fluorescence photons imposed by the paraffin. The fact that the area under the curve of each peak assigned by the software is smaller than it should be results in a smaller value for the concentration of the element correspondent to that peak.

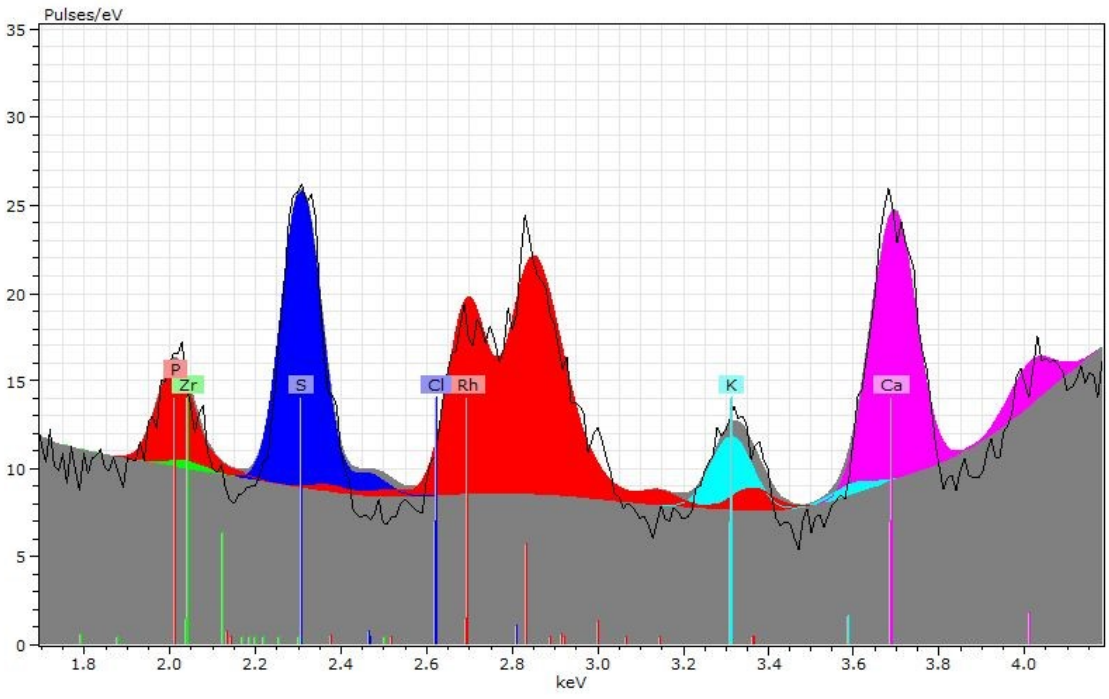

Figure 2.21: Sample 14 - Light elements spectrum (Al 12.5 μm filter).

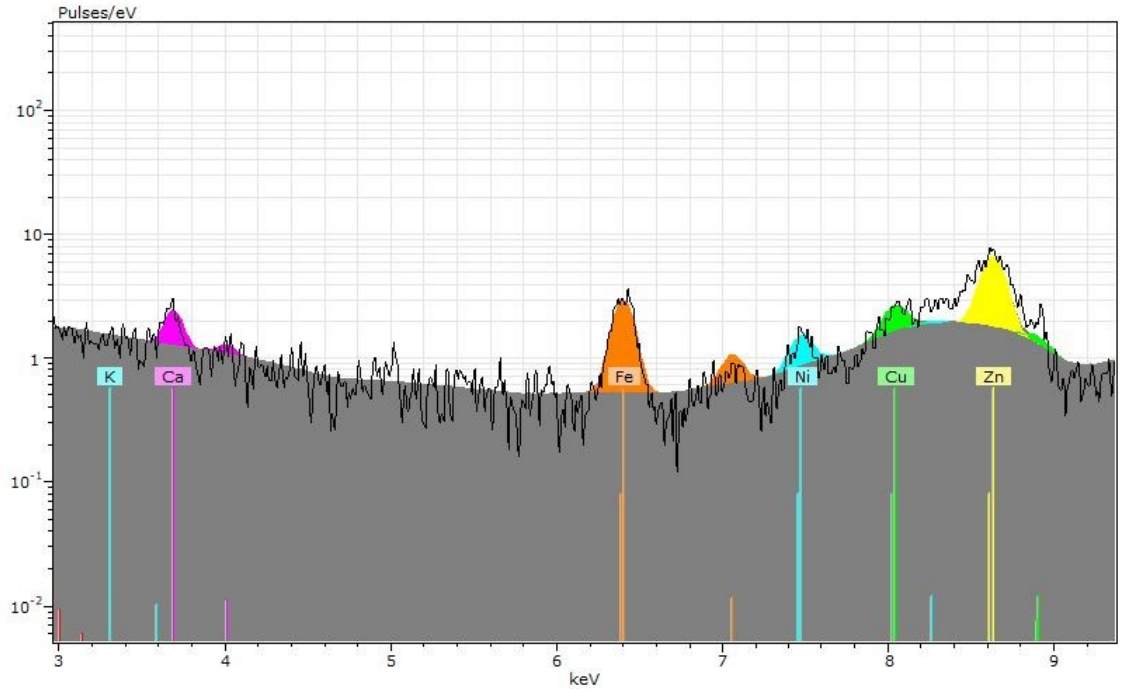

Figure 2.22: Sample 14 - Heavy elements spectrum (Al/Ti/Cu 100/50/25 μm filter).

To overcome this problem, the M4 Tornado software allows for the input of a quantification correction factor for each element. The calculation of these factors was done through the minimization of a cost function, in which the cost was the total deviation from the values obtained for the lyophilized samples. The obtained values were then rounded to the units to avoid overfitting and forced not to exceed 4. The chosen values for the correction factors for each analyzed element are shown in table 2.8.

Table 2.8: Correction factors.

P	S	Ca	Fe	Ni	Cu	Zn
3	3	2	4	1	2	4

The deviations of the quantification of the FFPE samples from their corresponding lyophilized sample after the application of the correction factors are shown in figures 2.23 and 2.24.

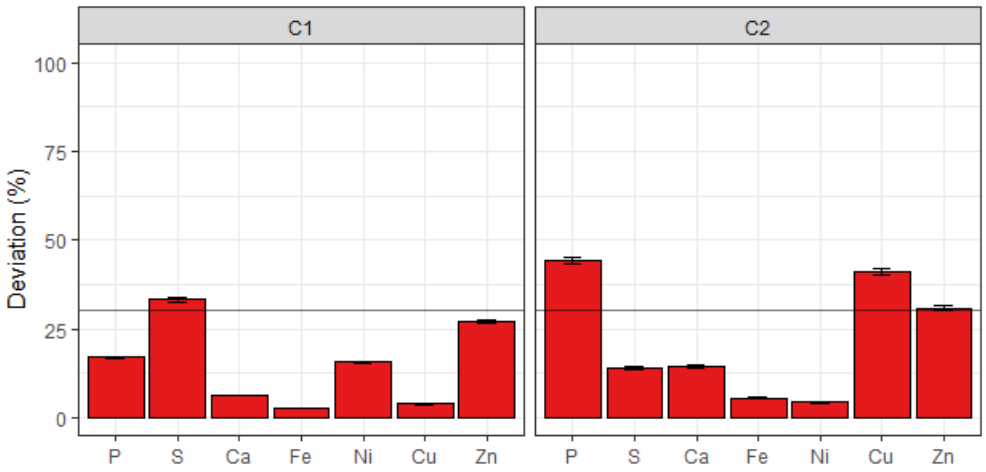

Figure 2.23: Deviations from reference values after the application of correction factors (in %) - Colon samples - Dark Matrix 1.

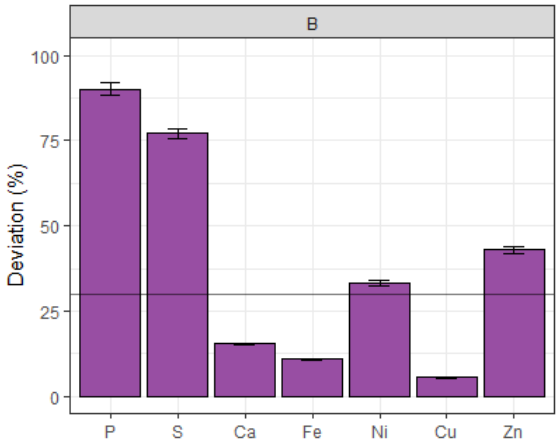

Figure 2.24: Deviations from reference values after the application of correction factors (in %) - Breast samples - Dark Matrix 4.

There is a clear improvement from the results shown in figure 2.20, but using the same factors for both breast and colon samples, it still wasn't possible to get all the elements' deviations from the reference values under 30%. It is important to note that even though the mirror pairs of samples used to validate these matrices were prepared using portions from the same organ and donor, they are not exactly the same portion of tissue, which is enough to produce significant differences in the concentration of these elements. The newly discovered influence of formalin in the concentration of the trace elements may also be responsible for the observed differences.

Also worth mentioning is the fact that the method for obtaining the reference values wasn't ideal. Given the remaining time available for the conclusion of this work after the

discovery of the influence of formalin in the concentration of the trace elements, it was the best option, but the number of samples was small, the formalin's influence wasn't totally removed, only attenuated, and even though DarkM has been shown to be accurate in quantifying lyophilized samples of human tissue [18], it has a degree of uncertainty, especially considering the fact that the same matrix was used for two different organs. Ideally, samples should have been fixed in formalin and then split - half to be analyzed in ICP-OES and the other half to be embedded in paraffin and analyzed with μEDXRF. This way, the influence of the formalin in the results would be minimal, since both groups of samples would have spent the same time in formalin.

Although the quantification method is not as accurate as required, for the purpose of this work, which is testing trace element's potential use as biomarkers for carcinogenesis, the uncertainty in the determinations of every tissue is assumed to be equal, so significant increase/decrease between normal/tumor. Since the difficulties imposed by the formalin and the paraffin are the same in the samples of both kinds of tissue, the comparison should still be reliable.

2.7 Statistical Analysis

The normality the distributions of each of the trace elements on each kind of tissue was tested with the Shapiro-Wilk Test. The results of this test showed that some elements were normally distributed and others weren't. Since not all elements were normally distributed, non-parametric tests were used to test for differences in the normal and tumor distributions, since they do not require the normality of the distributions.

Two non-parametric tests were used: the **Kruskal-Wallis Test** and the **Wilcoxon Test**. The Kruskal-Wallis Test infers differences in distributions based on the difference in the medians of those distributions. The Wilcoxon Test uses the difference between paired values in both distributions. It only makes sense to use this test in this context because the normal and tumor samples are paired, since they were taken from the same donor, otherwise the Wilcoxon Test could not be used. Both these tests' null hypothesis states that both distributions are alike, and can only be rejected if the p-value is inferior to 0.05, in which case, the alternative hypothesis is taken, meaning that there is a significant difference between the distributions.

3

Results and Discussion

3.1 Area Selection Tool: Approach A vs Approach B

Approach A was designed to exclude areas with only paraffin and no tissue in the sample. The obtained areas fulfilled that goal, as visible in the examples of figure 3.1.

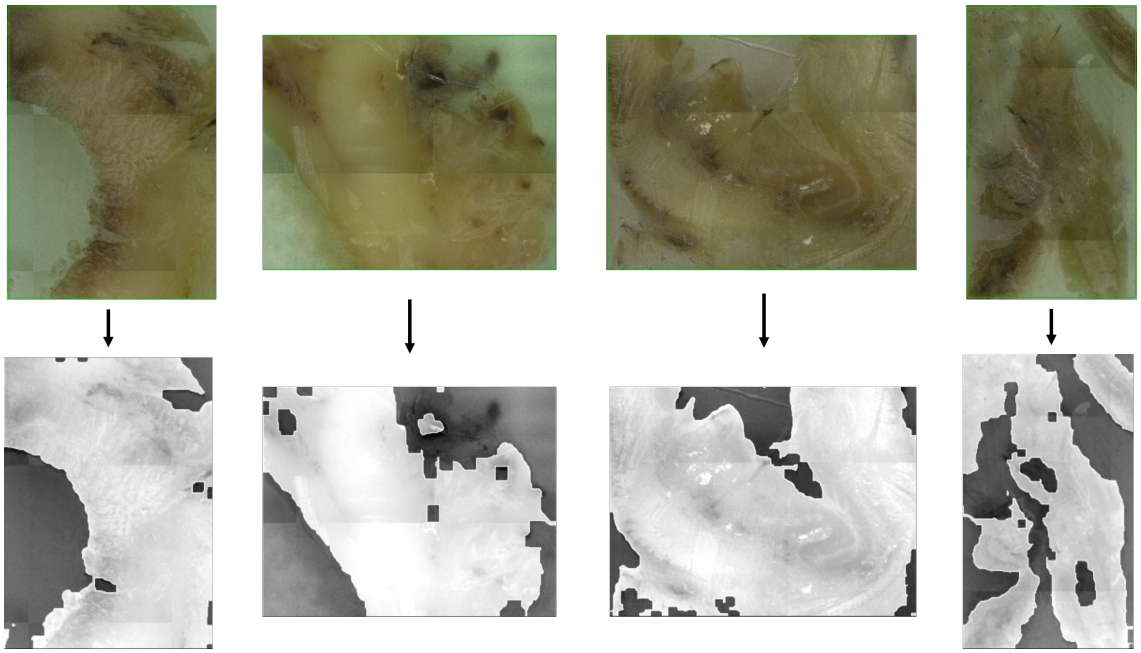

Figure 3.1: Examples of the output of area selection with Approach A in four different samples.

There are a few regions that are not selected and might contain tissue, but the regions selected contain tissue, and are good areas to extract spectra from. Since these areas were identified based on the sulfur mappings, it is likely that those regions of tissue that were not selected corresponded to areas with low concentration of sulfur, or with a thicker layer of paraffin, that attenuated the sulfur fluorescence photons more than in the neighboring selected regions.

Approach B was conceived to be an enhancement of approach A in avoiding the difficulties imposed by the paraffin, by targeting the areas thinner layers of paraffin over the tissue.

Through the use of Approach B, the results of quantification show higher values of S and P concentration relative to approach A as shown in figure 3.2. These elements were always greatly undervalued in both Dark Matrix determination attempts covered in chapter 2, being among the elements that made the difficulties imposed by the paraffin more evident.

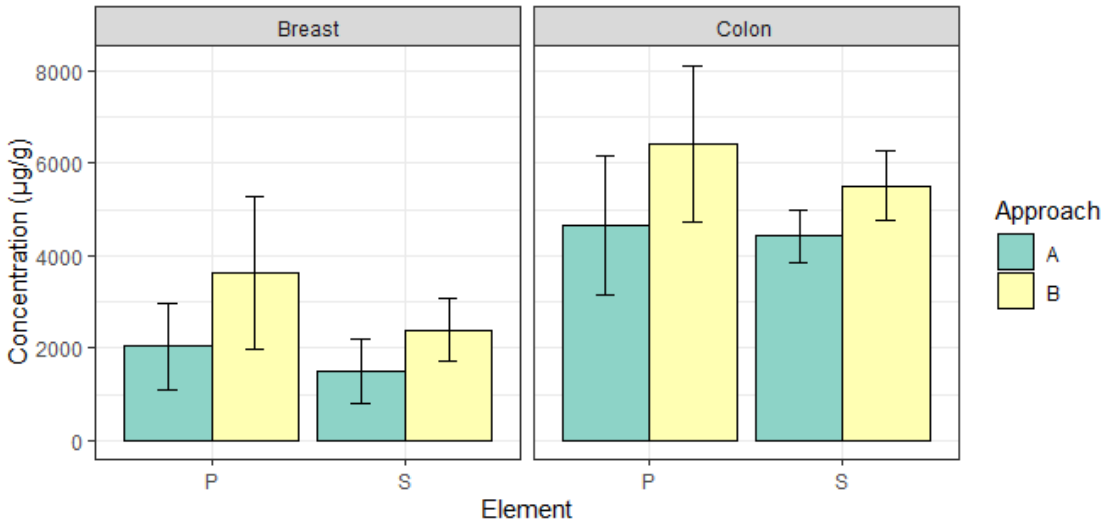

Figure 3.2: S and P quantification results with the use of the area selection approaches A and B.

The fact that results of quantification for these elements with Approach B show higher values, might be an indication that Approach B is effective in finding the areas of the sample with thinner layers of paraffin over the tissue.

However, this gave rise to a problem. The tumor samples do not contain exclusively tumor tissue. There is an unavoidable surgical margin of normal tissue that is also removed along with the tumor tissue and is present in the tumor samples. This means that there is a non-negligible probability that the area with the thinner layer of paraffin selected by Approach B resides over a portion of normal tissue of the tumor sample, which was later confirmed by Dr. José Vilchéz and Dr. Carlos Montenegro, the doctors responsible for providing the samples for this study. When shown the areas selected by both approaches, they stated that Approach B was selecting non-tumor regions of tumor samples in a significant number of cases. This reflected in the results obtained through Approach B when comparing normal and tumor tissue. Figure 3.3 shows a summary of the obtained results for colon and breast with Approach B.

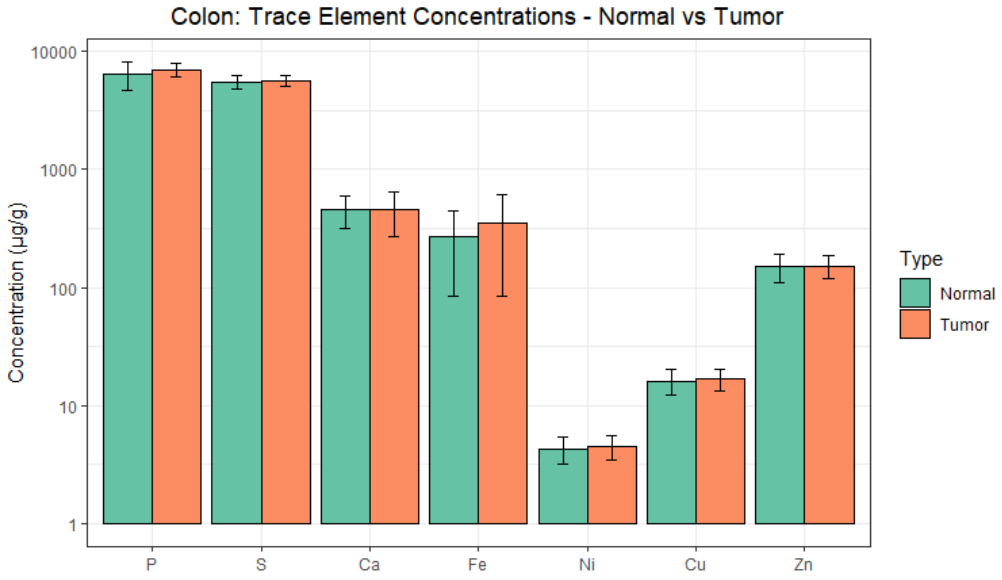

(a) Colon

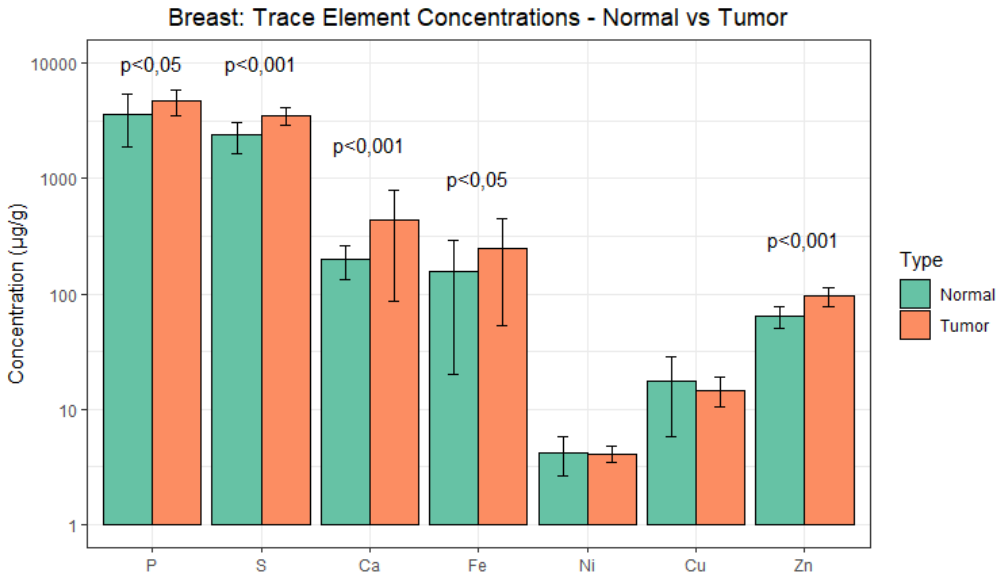

(b) Breast

Figure 3.3: Bar chart of the concentrations of the different trace elements in normal and tumor tissue for colon and breast using Approach B.

No significant difference between normal and tumor tissue was found in colon, unlike with Approach A as will be shown in section 3.2. For breast, the significance of the differences found was smaller than with Approach A.

For the reasons stated, Approach A was deemed more suited for comparing normal and tumor tissue, and was used to obtain the results presented in the next section.

3.2 Concentration of Trace Elements In Colon and Breast: Normal vs Tumor Tissue

The 30 pairs of colon samples and 28 pairs of breast samples were analyzed in the M4 Tornado spectrometer. The areas from which the spectrum was selected for quantification were chosen using Approach A. The Dark Matrix composition used for the quantitative analysis through the Fundamental Parameters Method was Dark Matrix 1 for the colon samples and Dark Matrix 4 for the breast samples.

In this section, the results of quantification of each element in normal and tumor tissue for colon and breast are shown in depicted in the form of box-plots and compared with the Kruskal-Wallis and Wilcoxon tests.

For each element, when a sample showed values that differed by an order of magnitude or more, the corresponding pair was considered an outlier, and was not depicted in the box-plot. The values shown in the tables also refer to the distributions after the remotion of the outlier pairs. The number of samples used in each comparison is presented in each table, in the column labelled "N". However, the statistical tests were always performed with the number of samples depicted in the boxplots (excluding the outliers), and also with the total number of samples (including the outliers). The differences found between the normal and tumor distributions were always the same in both conditions, and so was the significance of those differences.

3.2.1 Phosphorus

3.2.1.1 Colon

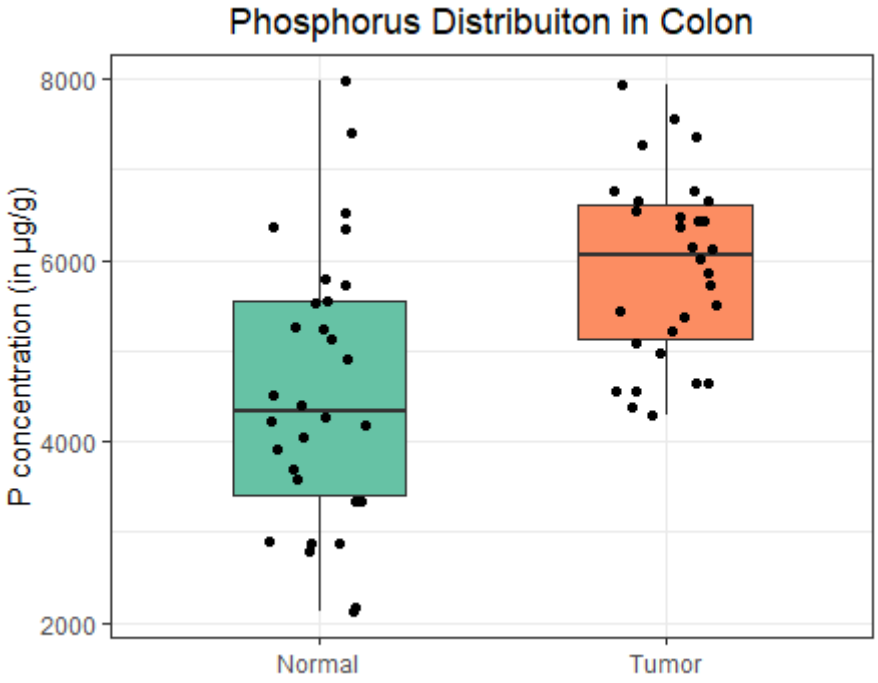

Figure 3.4: Box-plot of the concentration distributions of P in normal and tumor colon tissue.

Figure 3.4 shows box-plots comparing the obtained concentrations of phosphorus in normal and tumor tissue for colon. The range of values is wider in normal tissue than in tumor tissue. There is a very significant difference between the medians of the two distributions, both visible in figure 3.4, and on table 3.1. The significance of this difference is corroborated by the p-values of both statistical tests performed, which are lower than 0.001. This increase and the magnitude of the values obtained are in accordance with the results found by Magalhães et al. [24].

Table 3.1: Colon - statistical results for P distributions.

Element	Type	N	Median	Min	Max	p-value	
						Kruskal-Wallis	Wilcoxon
P	normal	30	4327.7	2127.9	7974.2	<0.001	<0.001
	tumor	30	6063.4	4294.6	7931.3		

3.2.1.2 Breast

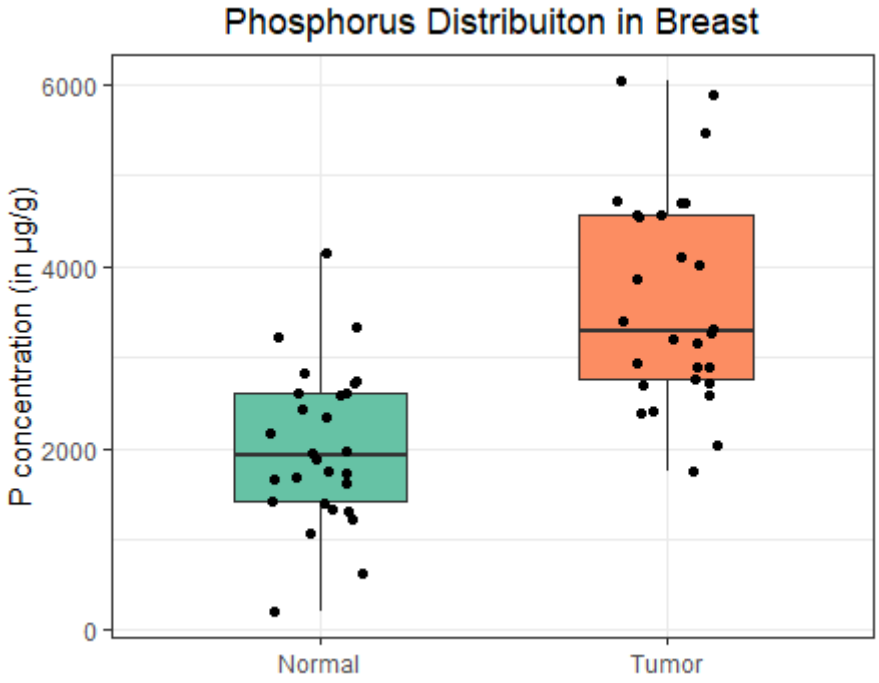

Figure 3.5: Box-plot of the concentration distributions of P in normal and tumor breast tissue.

Figure 3.5 shows box-plots comparing the obtained concentrations of phosphorus in normal and tumor tissue for breast. The range span similarly in normal and tumor tissue, which was not the case in colon, but the behaviour of the distributions is similar. There is a very significant increase in the median of the tumor distributions, both visible in figure 3.5 and on table 3.2. Similarly to colon, the significance of this difference is corroborated by the p-values of both statistical tests performed, which are lower than 0.001. This increase is in accordance with the results published by Magalhães et al. [24] and Machado et al [12]. The magnitude of the values obtained is also in accordance with the results found by Machado et al [12].

Table 3.2: Breast - statistical results for P distributions.

Element	Type	N	Median	Min	Max	p-value	
						Kruskal-Wallis	Wilcoxon
P	normal	28	1913.0	214.0	4134.0	<0.001	<0.001
	tumor	28	3284.7	1745.0	6027.3		

3.2.2 Sulfur

3.2.2.1 Colon

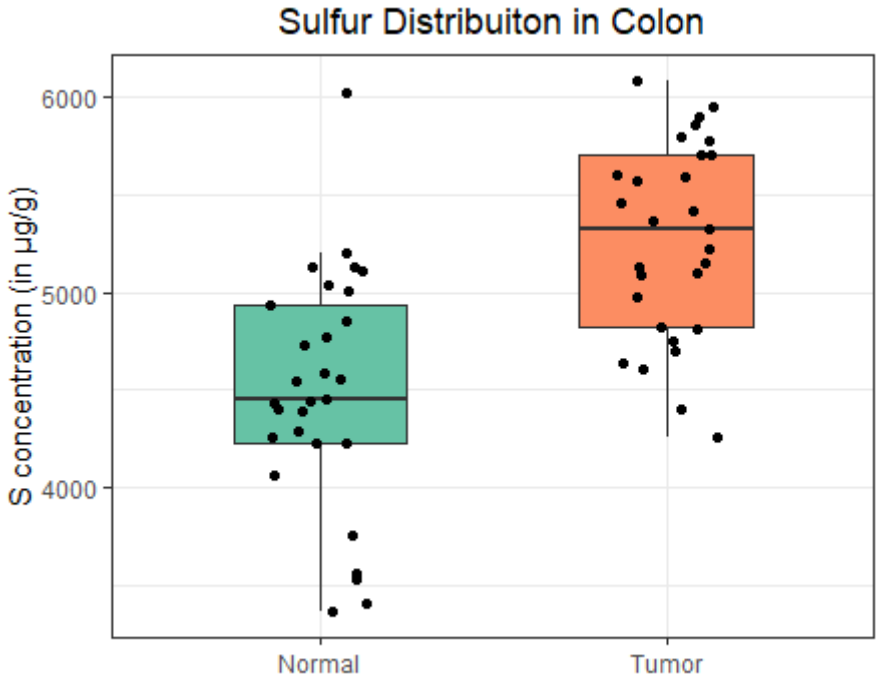

Figure 3.6: Box-plot of the concentration distributions of S in normal and tumor colon tissue.

Box-plots comparing the obtained concentrations of sulfur in normal and tumor tissue for colon is shown in figure 3.6. The behaviour shown is similar to that of P, with an increase of the concentration in tumor tissue relative to the normal tissue. The difference between the distributions in normal and tumor tissue is very significant, since the p-value obtained from both of the statistical tests is lower than 0.001.

The increase of concentration of S in tumor tissue relative to normal tissue and the magnitude of values are in accordance with the results found by Magalhães et al. [24].

Table 3.3: Colon - statistical results for S distributions.

Element	Type	N	Median	Min	Max	p-value	
						Kruskal-Wallis	Wilcoxon
S	normal	29	4455.2	3365.8	6023.8	<0.001	<0.001
	tumor	29	5331.0	4257.8	6083.8		

3.2.2.2 Breast

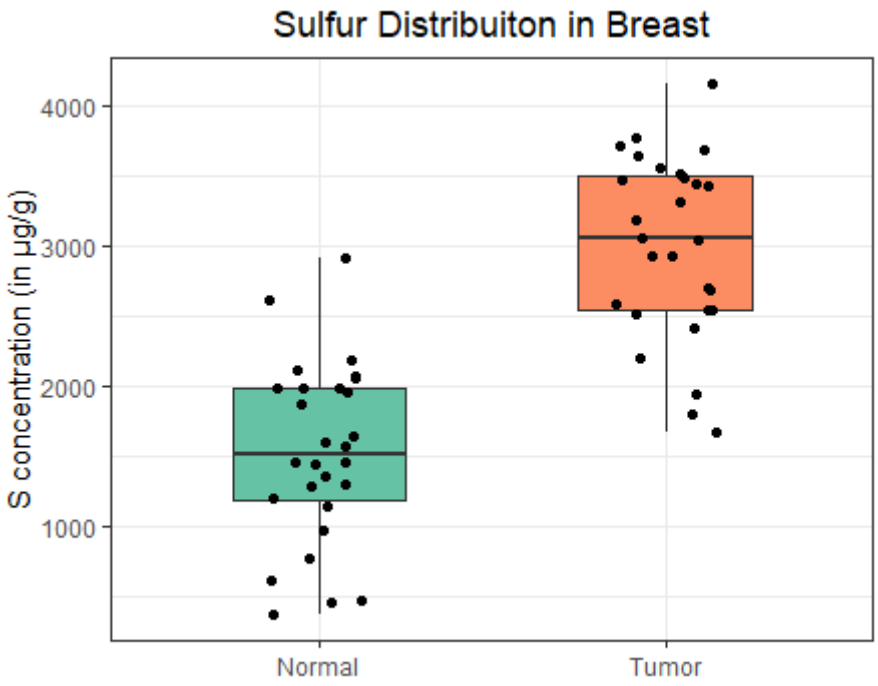

Figure 3.7: Box-plot of the concentration distributions of S in normal and tumor breast tissue.

Box-plots comparing the obtained concentrations of sulfur in normal and tumor tissue for breast is shown in figure 3.7. Similarly to what was shown in colon, the behaviour shown is similar to that of P, with an increase of the concentration in tumor tissue relative to the normal tissue. The difference between the distributions in normal and tumor tissue is also very significant, with the p-value obtained from both of the statistical tests being lower than 0.001.

The increase of concentration of S in tumor tissue relative to normal tissue is in accordance with the results found by Magalhães et al. [24] and Machado et al. [12].

Table 3.4: Breast - statistical results for S distributions.

Element	Type	N	Median	Min	Max	p-value	
						Kruskal-Wallis	Wilcoxon
S	normal	28	1517.8	378.2	2917.0	<0.001	<0.001
	tumor	28	3053.3	1677.6	4154.2		

3.2.3 Calcium

3.2.3.1 Colon

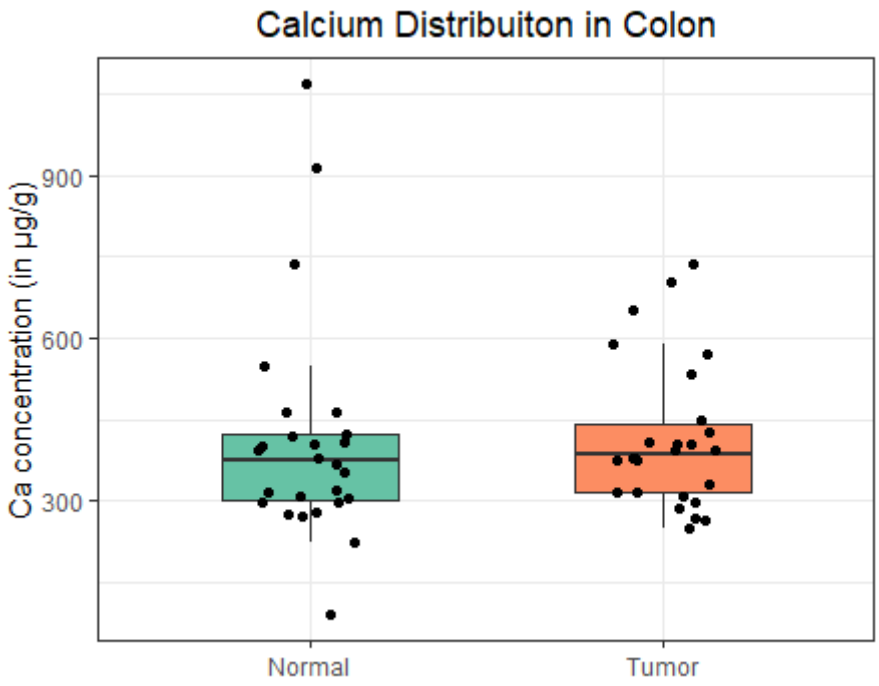

Figure 3.8: Box-plot of the concentration distributions of Ca in normal and tumor colon tissue.

In the case of colon, no significant difference was found between the calcium distributions in normal and tumor. Box-plots comparing the obtained concentrations are represented in figure 3.8. Since the p-values from both statistical tests presented on table 3.5 are higher than 0.05, the null hypothesis in the case of both tests can not be rejected, meaning that the distributions are similar.

Magalhães et al. [24] also found the concentration of Ca to be unchanged when comparing normal and tumor colon tissue.

Only 26 out of the 30 pairs of colon samples were considered. The four removed pairs showed concentrations over 10 times higher than the median, either in the normal or the tumor sample. The statistical tests were also performed without the removal of the outlier pairs and the p values were also both higher than 0.05.

Table 3.5: Colon - statistical results for Ca distributions.

Element	Type	N	Median	Min	Max	p-value	
						Kruskal-Wallis	Wilcoxon
Ca	normal	26	373.7	92.5	1066.6	0.287	0.088
	tumor	26	385.3	248.8	734.6		

3.2.3.2 Breast

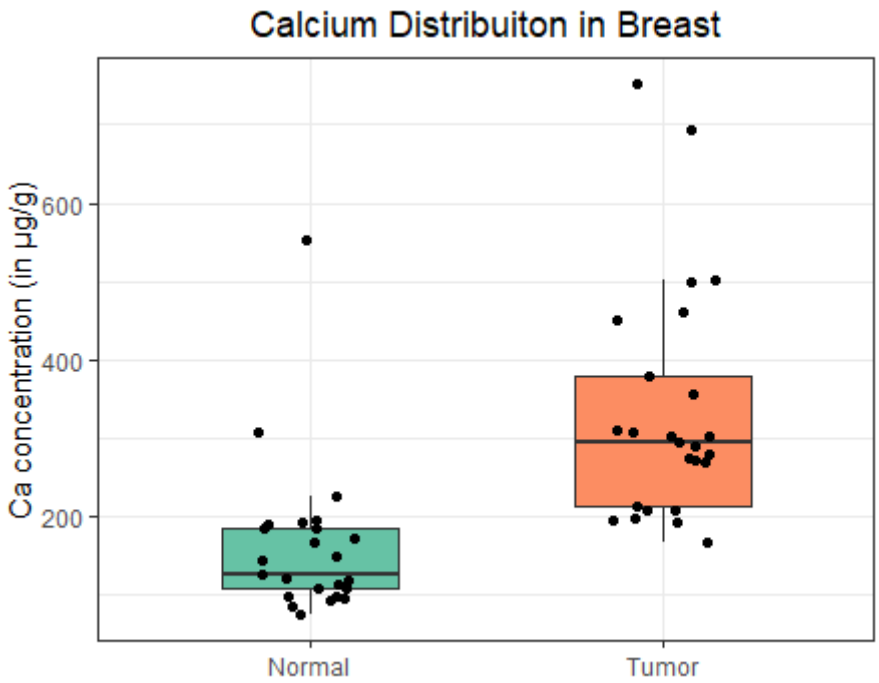

Figure 3.9: Box-plot of the concentration distributions of Ca in normal and tumor breast tissue.

Figure 3.9 shows box-plots comparing the obtained concentrations of calcium in normal and tumor breast tissue. There is a visible increase of calcium in tumor tissue when compared to normal tissue, which is supported by the p-values presented in table 3.6. Since the p-values provided by both statistical tests are below 0.001, the difference between the two distributions is very significant.

Similarly to colon, a few outlier pairs had to be disregarded for showing concentrations over 10 times higher than the median, either in the normal or the tumor sample. Only 25 out of the 30 pairs of breast samples were considered, however, the statistical tests were also performed without the removal of the outlier pairs and the p-values were also both lower than 0.001.

The increase in the concentration of Ca in tumor tissue breast when compared to normal breast tissue is in accordance with the results of Silva et al. [27] and Magalhães et al. [24].

Table 3.6: Breast - statistical results for Ca distributions.

Element	Type	N	Median	Min	Max	p-value	
						Kruskal-Wallis	Wilcoxon
Ca	normal	25	126.6	76.3	552.3	<0.001	<0.001
	tumor	25	295.4	168.0	751.8		

3.2.4 Iron

3.2.4.1 Colon

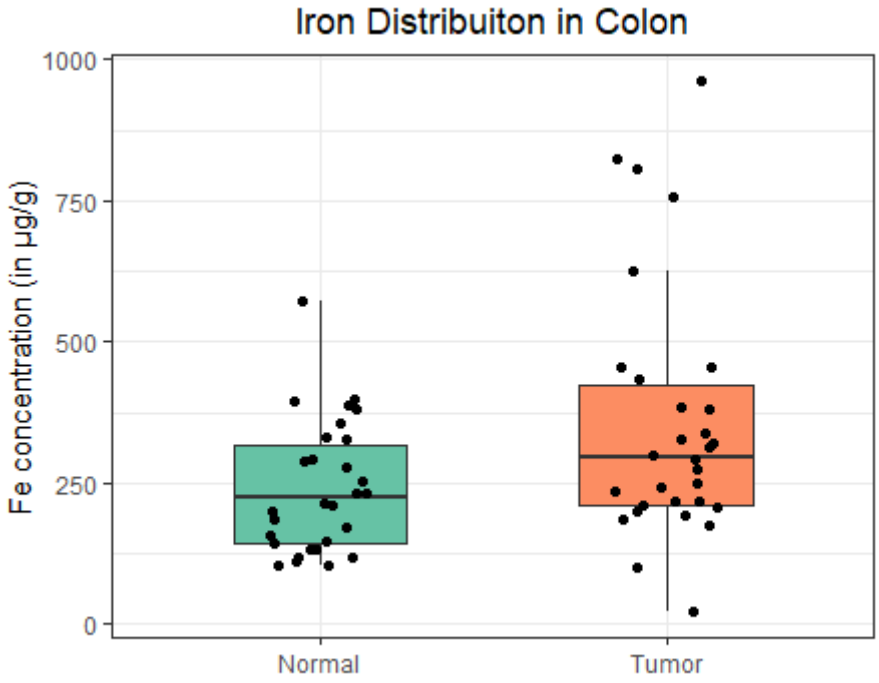

Figure 3.10: Box-plot of the concentration distributions of Fe in normal and tumor colon tissue.

Box-plots comparing the obtained concentrations ofiron in normal and tumor tissue for colon are shown in figure 3.10. The range of values is wider for the tumor tissue distribution as visible both in figure 3.10 and the values presented in table 3.7. There is a significant increase in the concentration of Fe in colon tumor tissue when compared to the normal tissue, since both p-values resultant form the two statistical tests used are lower than 0.05. This result is contrary to that found by Carvalho et al. [32].

Table 3.7: Colon - statistical results for Fe distributions.

Element	Type	N	Median	Min	Max	p-value	
						Kruskal-Wallis	Wilcoxon
Fe	normal	30	222.9	104.3	573.9	<0.05	<0.05
	tumor	30	297.0	23.3	961.5		

3.2.4.2 Breast

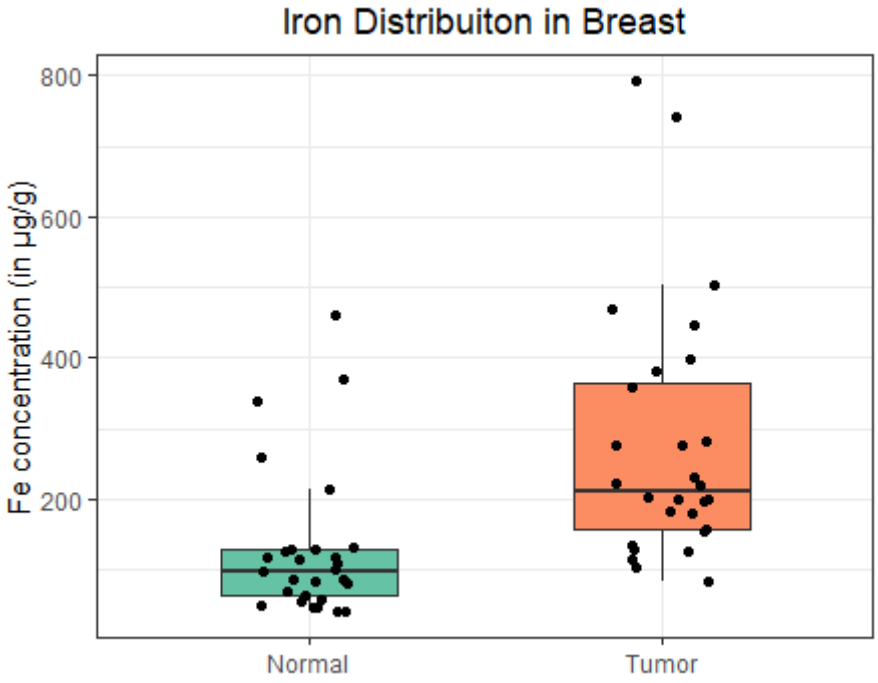

Figure 3.11: Box-plot of the concentration distributions of Fe in normal and tumor breast tissue.

Box-plots comparing the obtained concentrations of iron in normal and tumor tissue for breast are shown in figure 3.11. The behaviour of iron shown in breast is similar to the behaviour shown in colon. The range of values is wider for the tumor tissue distribution, and there is also an increase of concentration in tumor as visible both in figure 3.11 and the values presented in table 3.8. The increase, however is more significant, with both p-values resultant from the two statistical tests used being lower than 0.001.

Silva et al. [27] and Magalhães et al. [24] also found an increase in the concentration of iron in breast tumor tissue.

Table 3.8: Breast - statistical results for Fe distributions.

Element	Type	N	Median	Min	Max	p-value	
						Kruskal-Wallis	Wilcoxon
Fe	normal	28	98.4	41.2	461.1	<0.001	<0.001
	tumor	28	210.1	82.7	791.8		

3.2.5 Nickel

3.2.5.1 Colon

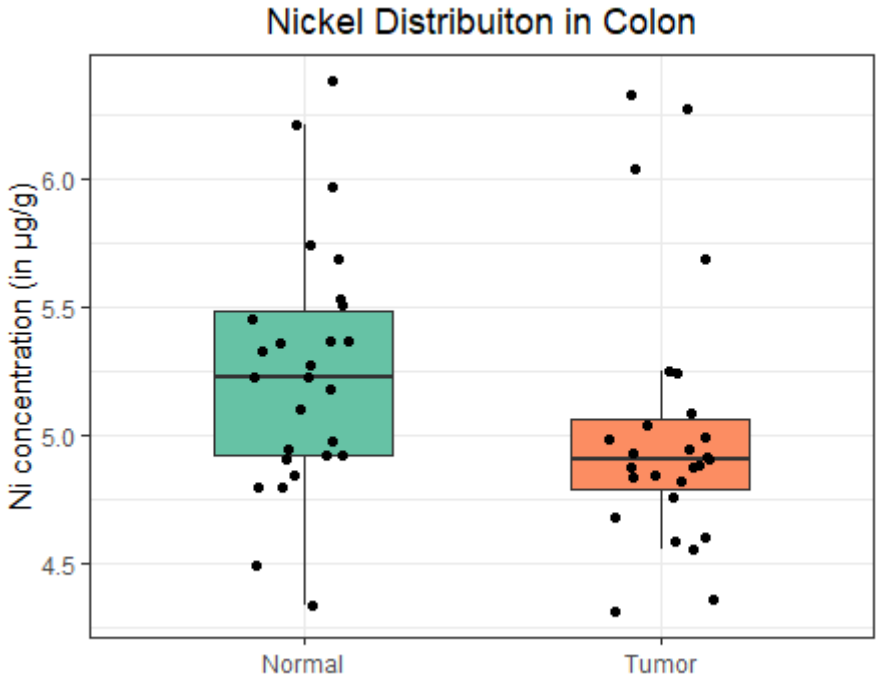

Figure 3.12: Box-plot of the concentration distributions of Ni in normal and tumor colon tissue.

Figure 3.12 shows box-plots comparing the obtained concentrations of nickel in normal and tumor colon tissue. A decrease in the concentration of nickel in colon tumor tissue as been found relative to the normal tissue. The p-values obtained through the use of both tests differs, being lower than 0,001 with the Wilcoxon test, but only lower than 0.05 with the Kruskal-Wallis test. Based on both p-values presented on table 3.9, both tests deem the decrease significant, but the level of significance is considered higher through the use of the Wilcoxon test.

Table 3.9: Colon - statistical results for Ni distributions.

Element	Type	N	Median	Min	Max	p-value	
						Kruskal-Wallis	Wilcoxon
Ni	normal	27	5.2	4.3	6.4	<0.05	<0.001
	tumor	27	4.9	4.3	6.3		

3.2.5.2 Breast

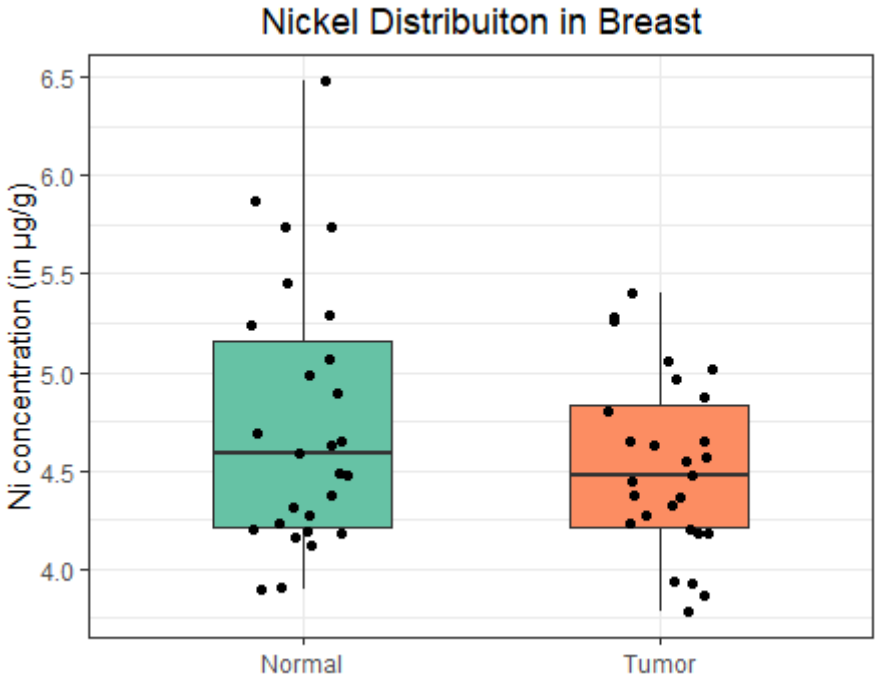

Figure 3.13: Box-plot of the concentration distributions of Ni in normal and tumor breast tissue.

Figure 3.13 shows box-plots comparing the obtained concentrations of nickel in normal and tumor breast tissue. Other than the different slightly different width in the range of values, no significant difference was found between both distributions, since both p-values presented in table 3.10 are higher than 0.05.

Magalhães et al. have found an increase in the concentration of Ni in breast tumor tissue [24]. It is possible that the reason for the absence of difference in the distributions observed is due to the small concentration in the tissue and its presence on the paraffin.

Table 3.10: Breast - statistical results for Ni distributions.

Element	Type	N	Median	Min	Max	p-value	
						Kruskal-Wallis	Wilcoxon
Ni	normal	27	4.6	3.9	6.5	0.326	0.126
	tumor	27	4.5	3.8	5.4		

3.2.6 Copper

3.2.6.1 Colon

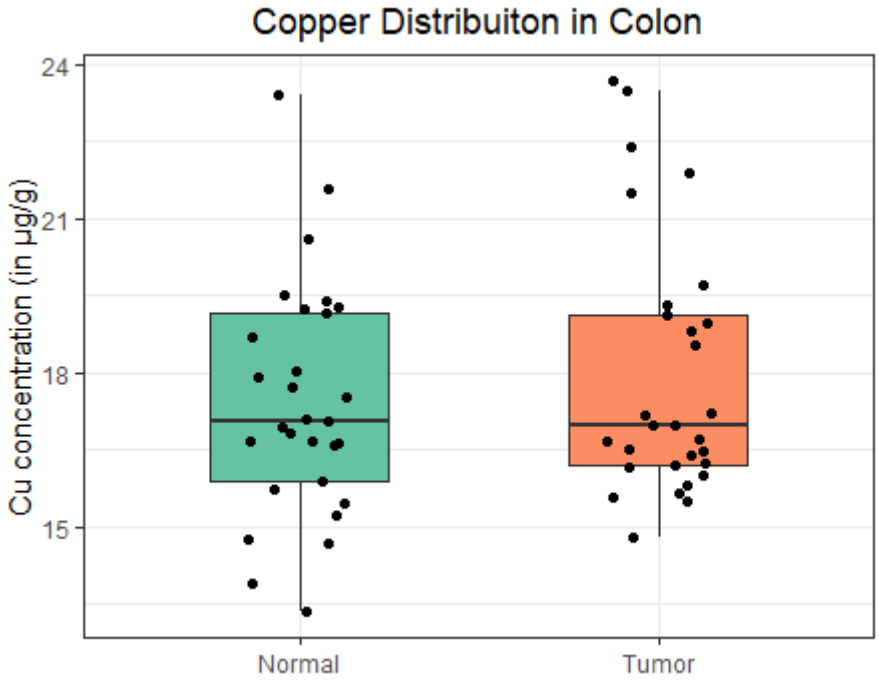

Figure 3.14: Box-plot of the concentration distributions of Cu in normal and tumor colon tissue.

Box-plots comparing the obtained concentrations of copper in normal and tumor tissue for colon are shown in figure 3.14. Since the p-values from both statistical tests presented on table 3.5 are higher than 0.05, the null hypothesis in the case of both tests can not be rejected, meaning that the distributions are similar.

The literature isn't consensual about the behaviour of copper in colon tissue. Carvalho et al. [32] found a decrease in colon concentration, while Magalhães et al. found an increase of copper in tumor tissue [24]. Nonetheless, since this element is present in the paraffin and its concentration is low in the tissue, the expected result was for the measured concentrations in the normal and tumor samples to be similar, since the major copper contribution comes from the paraffin, which is the same in both samples.

Table 3.11: Colon - statistical results for Cu distributions.

Element	Type	N	Median	Min	Max	p-value	
						Kruskal-Wallis	Wilcoxon
Cu	normal	29	17.1	13.4	23.4	0.750	0.565
	tumor	29	17.0	14.8	23.7		

3.2.6.2 Breast

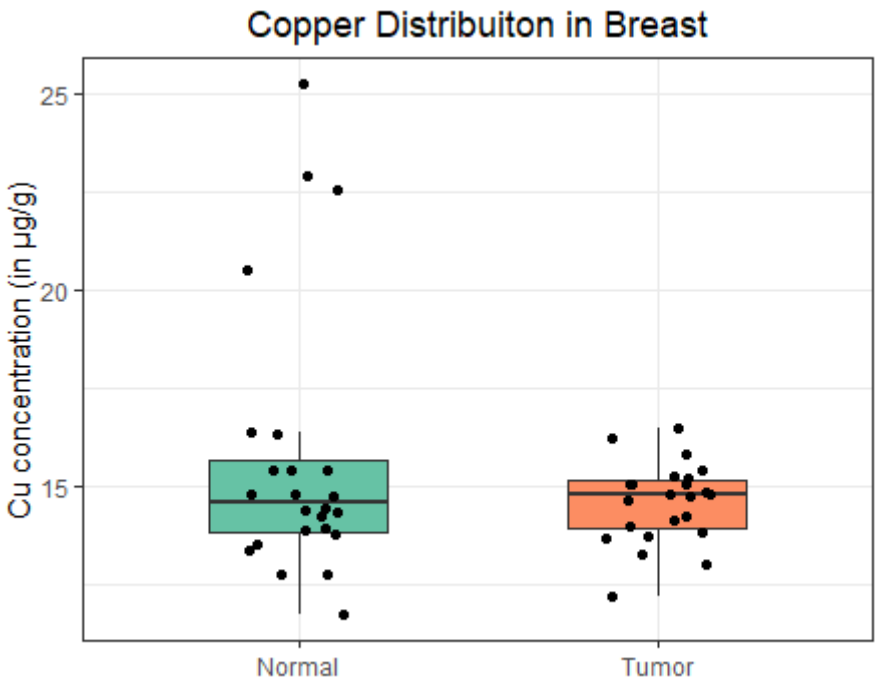

Figure 3.15: Box-plot of the concentration distributions of Cu in normal and tumor breast tissue.

Box-plots comparing the obtained concentrations of copper in normal and tumor breast tissue are shown in figure 3.15. Similarly to colon, the p-values from both statistical tests presented on table 3.5 are higher than 0.05, so the null hypothesis can not be rejected in either test, meaning that the distributions are similar. A considerable number of outliers was removed (5 out of 28 sample pairs), but both p-values were still higher than 0.05 before their removal.

The literature shows that the copper concentration tends to increase in tumor tissue [22–24, 27–29], but similarly to what was verified with colon, since this element is present in the paraffin and its concentration is low in the tissue, the expected result was for the measured concentrations in the normal and tumor samples to be similar, since the major copper contribution comes from the paraffin, which is the same in both samples.

Table 3.12: Breast - statistical results for Cu distributions.

Element	Type	N	Median	Min	Max	p-value	
						Kruskal-Wallis	Wilcoxon
Cu	normal	23	14.6	11.7	25.2	0.781	0.053
	tumor	23	14.8	12.2	119.7		

3.2.7 Zinc

3.2.7.1 Colon

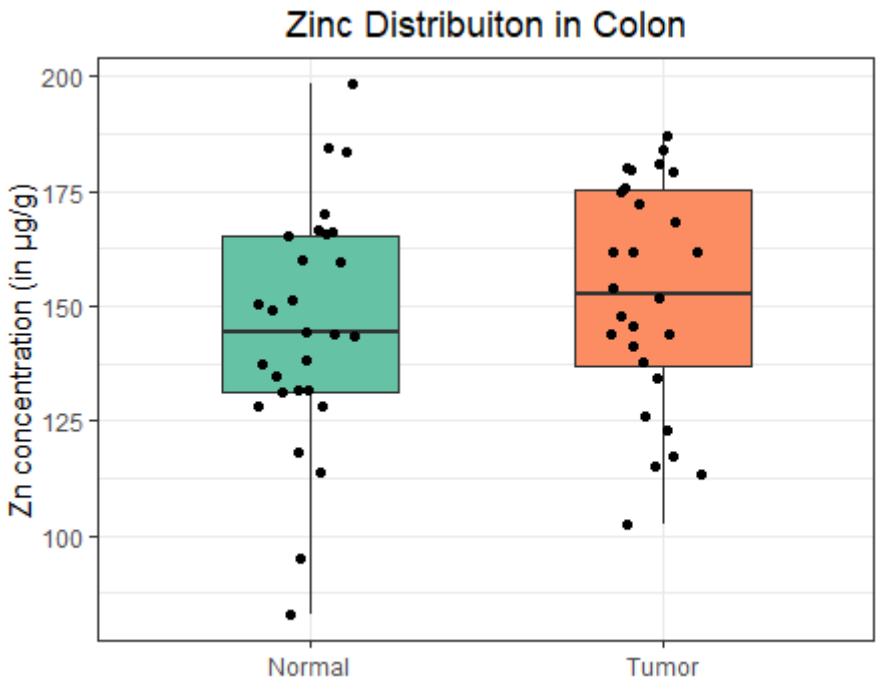

Figure 3.16: Box-plot of the concentration distributions of Zn in normal and tumor colon tissue.

Figure 3.16 shows box-plots comparing the obtained concentrations of zinc in normal and tumor colon tissue. No significant changes between both distributions was found, since the p-values obtained through the use of both tests presented on table 3.13 are higher than 0.05.

Magalhães et al. found an increase in the concentration of Zn in tumor tissue [24], while Carvalho et al, found a decrease in concentration of this element in tumor tissue when compared to the normal colon tissue [32]. None of these results match the ones obtained in this work.

Table 3.13: Colon - statistical results for Zn distributions.

Element	Type	N	Median	Min	Max	p-value	
						Kruskal-Wallis	Wilcoxon
Zn	normal	28	144.2	82.9	198.3	0.506	0.428
	tumor	28	152.7	102.4	187.3		

3.2.7.2 Breast

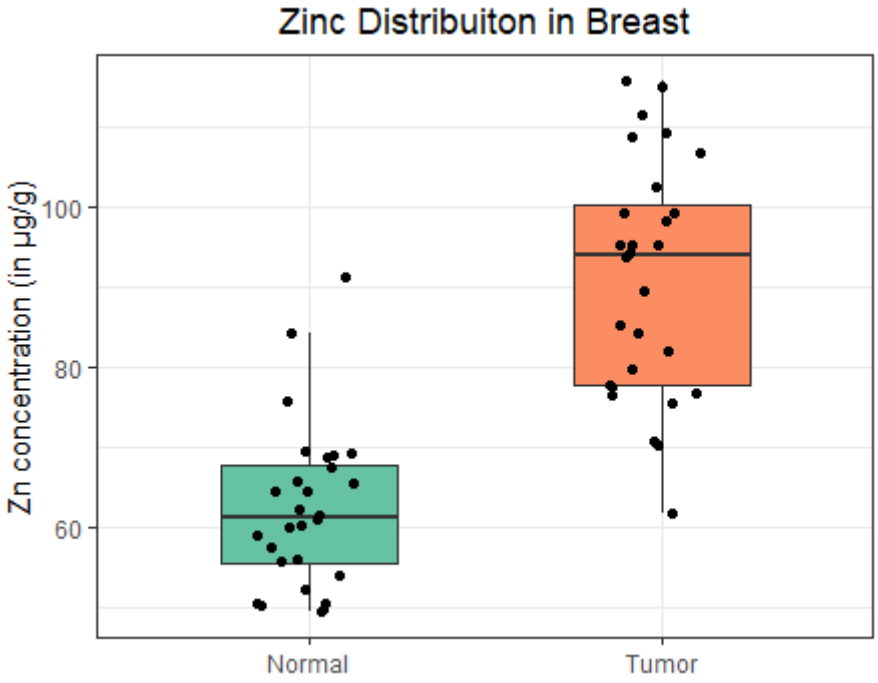

Figure 3.17: Box-plot of the concentration distributions of Zn in normal and tumor breast tissue.

Figure 3.16 shows box-plots comparing the obtained concentrations of zinc in normal and tumor breast tissue. There is a very significant difference between the medians of the two distributions, both visible in figure 3.4, and on table 3.1. The significance of this difference is corroborated by the p-values of both statistical tests performed, which are lower than 0.001.

The observed increase of Zn concentration breast tumor tissue is in accordance with the analyzed literature [22–24, 27–29].

Table 3.14: Breast - statistical results for Zn distributions.

Element	Type	N	Median	Min	Max	p-value	
						Kruskal-Wallis	Wilcoxon
Zn	normal	28	61.3	49.7	91.1	<0.001	<0.001
	tumor	28	94.0	61.8	115.5		

3.2.8 Summary

3.2.8.1 Colon

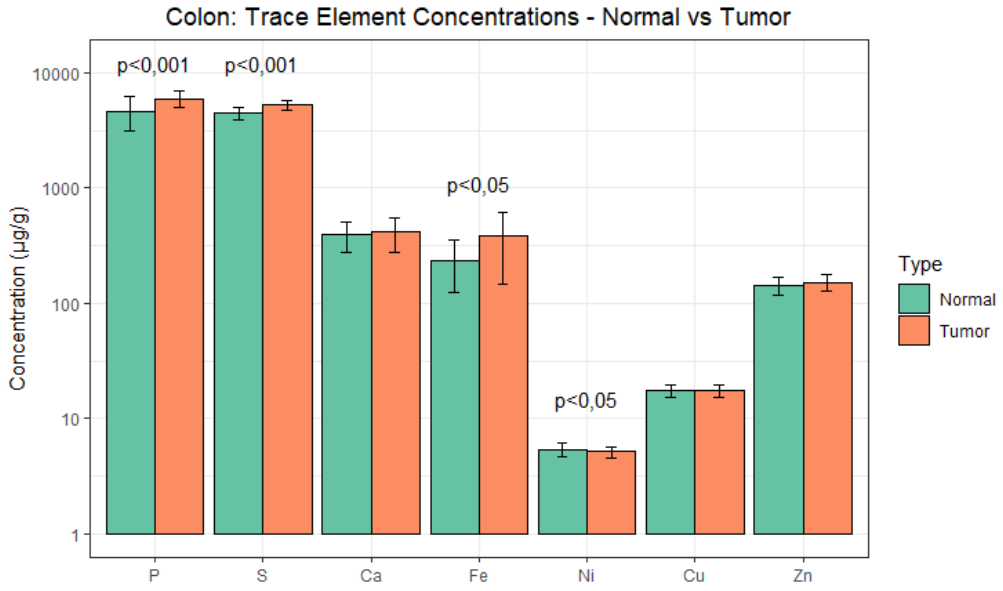

Figure 3.18: Summary: Bar chart of the concentrations of the different trace elements in normal and tumor colon tissue.

The p-values resultant form both the Kruskal-Wallis and the Wilcoxon tests were in agreement for all elements analyzed regarding the significance of the differences between the distributions of their concentration in normal and tumor tissue. In the case of Ni, both tests agreed that the change in concentration was significant, but the degree of significance was higher with the Wilcoxon test.

The results depicted in figure 3.18 show very significant increases in P and S, a significant increase in Fe and a significant decrease in Ni in tumor tissue when compared to normal tissue. The remaining elements show no changes.

The findings regarding P, S and Ca are in accordance with the analyzed literature. The only contrary result found was in the case of Fe, in which Carvalho et al. found a decrease in tumor [32]. As for the other elements, there is either no consensus in the literature (in the cases of Cu and Zn) or there was no information available (Ni). The reduced number of studies on this subject and the existence of contradictory results highlights the need of more studies with a larger number of samples.

According to these results, P and S can likely be used as tumor biomarkers in colon tissue. It is possible that Fe can too, but more research on the matter is needed to confirm. The observed increase makes sense, considering the presence of iron in hemoglobin and the fact that tumor tissue has a large amount of blood vessels, but the fact that Carvalho et al. found contrary results raises doubts. As for Ni, despite the significant decrease observed, due to its presence in the paraffin and its low concentration in the tissue, it

is possible that the decrease is statistical and due to the paraffin. Since no information regarding Ni in colon was found in the literature, more research is needed.

3.2.8.2 Breast

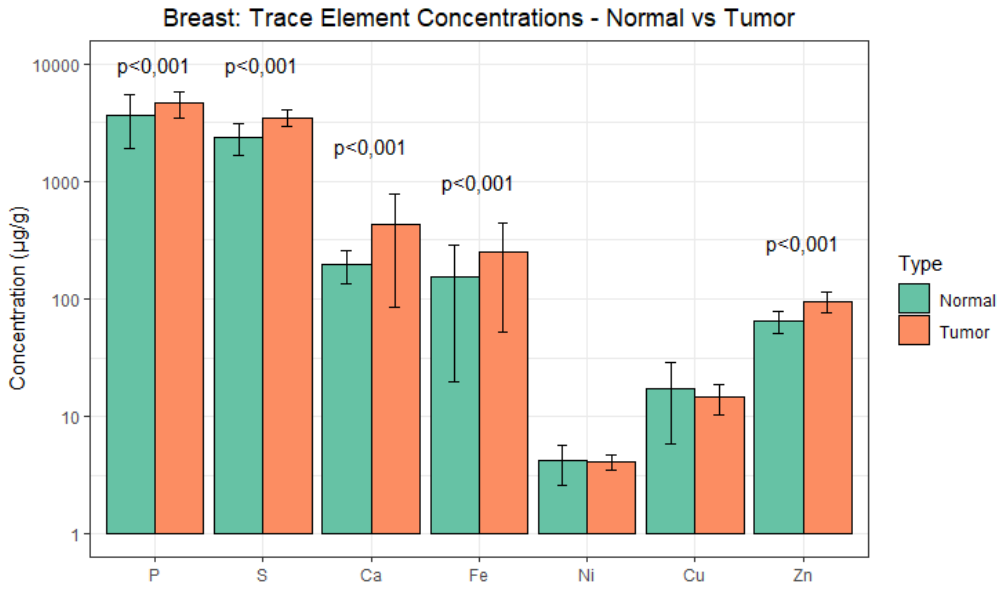

Figure 3.19: Summary: Bar chart of the concentrations of the different trace elements in normal and tumor breast tissue.

The results obtained for show the suitability of the selected matrix for the comparative analysis of breast normal and tumor tissue. The p-values resultant form both the Kruskal-Wallis and the Wilcoxon tests were in agreement for all elements analyzed regarding the significance of the differences between the distributions of their concentration in normal and tumor tissue.

The results depicted in figure 3.19 show very significant increases in P, S, Ca, Fe and Zn in tumor tissue when compared to normal tissue. Ni and Cu showed no changes.

All the changes found between normal and tumor breast tissue are in accordance with the analyzed literature. The only incongruities were in Ni and Cu, where the literature reports these elements' concentration should increase in tumor tissue, but no change was found in this work. The fact that no change between the concentrations of Ni and Cu in normal and tumor tissue was found is likely due to the presence of these elements in the paraffin and low concentration in the tissue.

Based on the obtained results, P, S, Ca, Fe and Zn can all likely be used as tumor biomarkers in breast tissue.

4

Conclusions

The methods chosen for this work are promising in the context of investigating trace elements' potential use as biomarkers for carcinogenesis.

Despite the problems faced due to the formalin and the paraffin, the use of FFPE samples allowed for the number of samples used in this work to be much higher than other studies of this kind.

The area selection tool developed in R was able to successfully identify the areas of the paraffin blocks that contained the tissue. The μEDXRF analysis has shown to be suitable, since it was possible to detect differences between normal and tumor tissue with the use of the Fundamental Parameters Method and the Dark Matrix compositions for colon and breast in accordance with the analyzed literature for most of the elements.

The method is still not yet accurate enough to compete with other quantitative analysis methods employed, but its non-destructive nature makes it a potentially useful contribution to the fields of physics and medicine.

The fact that the concentrations of Cl and K decreased significantly after a few days in formalin fixation indicate that this method might not be suitable for the quantification of these elements in FFPE samples.

In colon tissue, the elements that were found to be potential tumor biomarkers are P and S. Despite the changes also observed Fe and Ni, more research is needed to confirm their role in carcinogenesis. As for breast tissue, the elements that were found to be potential tumor biomarkers are P, S, Ca, Fe and Zn.

4.1 Future Work

One of the main obstacles faced in this work was the influence of the formalin in the concentration of the trace elements in the samples. It would be interesting to parametrize the nature of this influence, and the impact it has on the different elements. This could be achieved by having portions of tissue fixed in formalin for different periods of time, and measuring the evolution of the concentration of these elements in the tissue and also in the formalin.

Another obstacle that still needs to be overcome is the poor fit to the spectra obtained using the inbuilt software of the M4Tornado system due to the poor signal to noise ratio caused by the difficulties in detecting the fluorescence photons imposed by the paraffin. This could be done by developing a new software for spectra deconvolution and a quantification code, considering the difficulties of developing such a code for a commercial system.

It would also be important to improve the tool to identify the tumor regions in the tumor samples. Maybe with the collaboration of doctors and through the use of machine learning and image recognition algorithms. If the tumor areas are correctly identified, an area selection strategy similar to Approach B could potentially be an option to overcome the problems imposed by the paraffin.

An aspect that can be taken a step further in future works is the use of the spatial information provided by the mappings of each element. In this work it was only used to distinguish areas of the FFPE that had tissue from those that had only paraffin (through Approach A), but there is more that can be done. It would be interesting to compare the information in the mappings with digital microscopic imaging and try to establish connections between the spacial distribution of certain trace elements with the structure of the tissue at a cellular level.

Bibliography

[1] J. M. Lourenço. *The NOVAthesis LaTeX Template User's Manual*. NOVA University Lisbon. 2021. URL: https://github.com/joaomlourenco/novathesis/raw/master/template.pdf (cit. on p. iii).

[2] *"World Health Organization Website - Health Topics - Cancer"Accessed January 27, 2021*. URL: https://www.who.int/health-topics/cancer (cit. on p. 1).

[3] C. G. Fraga. "Relevance, essentiality and toxicity of trace elements in human health". In: *Molecular Aspects of Medicine* 26.4-5 (Aug. 2005). doi = 10.1016/j.mam.2005.07.013, pp. 235–244. ISSN: 00982997. URL: https://linkinghub.elsevier.com/retrieve/pii/S0098299705000464 (cit. on p. 2).

[4] P. J. Parsons and F. Barbosa. "Atomic spectrometry and trends in clinical laboratory medicine". In: *Spectrochimica Acta - Part B Atomic Spectroscopy* 62.9 (2007), pp. 992–1003. ISSN: 05848547. DOI: 10.1016/j.sab.2007.03.007 (cit. on p. 2).

[5] A. Taylor. "Detection and monitoring of disorders of essential trace elements". In: *Annals of Clinical Biochemistry* 33.6 (1996), pp. 486–510. ISSN: 00045632. DOI: 10.1177/000456329603300603 (cit. on p. 2).

[6] A. Taylor et al. "Atomic spectrometry update. Clinical and biological materials, foods and beverages". In: *J. Anal. At. Spectrom.* 19 (4 2004), pp. 505–556. DOI: 10.1039/B401305K. URL: http://dx.doi.org/10.1039/B401305K (cit. on p. 2).

[7] S. Tao. "Rigid motion correction for head CT imaging". PhD thesis. Department of Imaging and Pathology, Faculty of Medicine, KU Leuven Doctoral School Biomedical Sciences, Leuven, Feb. 2018, p. 8 (cit. on p. 3).

[8] E. P. Bertin. *Principles and practice of x-ray spectrometric analysis*. 2nd. Springer, 1975, pp. 6–84 (cit. on pp. 3, 4).

[9] J. H. Hubbell. "Compilation of Photon Cross-Sections: Some Historical Remarks and Current Status". In: *X-Ray Spectrometry* 28.4 (1999), pp. 215–223. ISSN: 00498246. DOI: 10.1002/(SICI)1097-4539(199907/08)28:4<215::AID-XRS336>3.0.CO;2-5 (cit. on p. 4).

[10] V. D. Hodoroaba and V. Rackwitz. "Gaining improved chemical composition by exploitation of compton-to-rayleigh intensity ratio in XRF analysis". In: *Analytical Chemistry* 86.14 (2014), pp. 6858–6864. ISSN: 15206882. DOI: 10.1021/ac5000619 (cit. on p. 4).

[11] S. Pessanha et al. "Suitability of the Compton-to-Rayleigh ratio in X-ray fluorescence spectroscopy: Hydroxyapatite-based materials characterization". In: *Journal of Analytical Atomic Spectrometry* 34.5 (2019), pp. 854–859. ISSN: 13645544. DOI: 10.1039/c8ja00370j (cit. on pp. 4, 25).

[12] J. Machado et al. "Accuracy improvement in XRF analysis for the quantification of elements ranging from tenths to thousands μg g-1in human tissues using different matrix reference materials". In: *Journal of Analytical Atomic Spectrometry* 35.12 (2020), pp. 2920–2927. ISSN: 13645544. DOI: 10.1039/d0ja00307g (cit. on pp. 4, 9, 39, 41).

[13] A. Puglisi. "Ab-initio study of x-ray spectroscopy of molecular ions". PhD thesis. Universite Pierre et Marie Curie, Paris, Sept. 2017, p. 26 (cit. on p. 5).

[14] F. Rouessac and A. Rouessac. *Chemical Analysis: Modern Instrumentation Methods and Techniques*. John Wiley & Sons, Ltd, 2007, p. 264 (cit. on p. 6).

[15] R. Sitko and B. Zawisza. "Quantification in X-Ray Fluorescence Spectrometry". In: *X-Ray Spectroscopy*. Ed. by S. K. Sharma. doi = 10.5772/29367. Rijeka: IntechOpen, 2012. Chap. 8. URL: https://doi.org/10.5772/29367 (cit. on pp. 7, 8).

[16] *"NIST - X-Ray Transition Energies Database"Accessed February 10, 2021*. URL: https://physics.nist.gov/PhysRefData/XrayTrans/Html/search.html (cit. on pp. 7, 8).

[17] S. Pessanha et al. "Comparison of standard-based and standardless methods of quantification used in X-ray fluorescence analysis: Application to the exoskeleton of clams". In: *X-Ray Spectrometry* 47.2 (Mar. 2018). doi = 10.1002/xrs.2819, pp. 108–115. ISSN: 00498246. URL: http://doi.wiley.com/10.1002/xrs.2819 (cit. on pp. 8, 9).

[18] A. Ensina et al. "Analysis of human tissues using Energy Dispersive X Ray Fluorescence – Dark matrix determination for the application to cancer research". In: *Journal of Trace Elements in Medicine and Biology* 68.June (2021). ISSN: 18783252. DOI: 10.1016/j.jtemb.2021.126837 (cit. on pp. 8, 10, 20, 24, 28, 33).

[19] R. Sitko. "Quantitative X-ray fluorescence analysis of samples of less than 'infinite thickness': Difficulties and possibilities". In: *Spectrochimica Acta - Part B Atomic Spectroscopy* 64.11-12 (2009), pp. 1161–1172. ISSN: 05848547. DOI: 10.1016/j.sab.2009.09.005 (cit. on p. 8).

[20] S. Akbulut. "Validation of classical quantitative fundamental parameters method using multivariate calibration procedures for trace element analysis in ED-XRF". In: *Journal of Analytical Atomic Spectrometry* 29.5 (2014), pp. 853–860. ISSN: 13645544. DOI: 10.1039/c3ja50377a (cit. on p. 8).

[21] T. Magalhães et al. "Trace elements in human cancerous and healthy tissues from the same individual: A comparative study by TXRF and EDXRF". In: *Spectrochimica Acta Part B: Atomic Spectroscopy* 61.10-11 (Nov. 2006). doi = 10.1016/j.sab.2006.06.002, pp. 1185–1193. ISSN: 05848547. URL: https://linkinghub.elsevier.com/retrieve/pii/S0584854706001716 (cit. on p. 9).

[22] M. Piacenti da Silva et al. "Discriminant analysis of trace elements in normal, benign and malignant breast tissues measured by total reflection X-ray fluorescence". In: *Spectrochimica Acta Part B: Atomic Spectroscopy* 64.6 (June 2009). doi = 10.1016/j.sab.2009.05.026, pp. 587–592. ISSN: 05848547. URL: https://linkinghub.elsevier.com/retrieve/pii/S058485470900130X (cit. on pp. 9, 49, 51).

[23] T. Magalhães et al. "Study of Br, Zn, Cu and Fe concentrations in healthy and cancer breast tissues by TXRF". In: *Spectrochimica Acta Part B: Atomic Spectroscopy* 63.12 (Dec. 2008). doi = 10.1016/j.sab.2008.10.014, pp. 1473–1479. ISSN: 05848547. URL: https://linkinghub.elsevier.com/retrieve/pii/S0584854708002851 (cit. on pp. 9, 49, 51).

[24] T. Magalhães et al. "Study on trace elements behaviour in cancerous and healthy tissues of colon, breast and stomach: Total reflection X-ray fluorescence applications". In: *Spectrochimica Acta Part B: Atomic Spectroscopy* 65.6 (June 2010). doi = 10.1016/j.sab.2010.04.001, pp. 493–498. ISSN: 05848547. URL: https://linkinghub.elsevier.com/retrieve/pii/S0584854710001126 (cit. on pp. 9, 10, 38–43, 45, 47–51).

[25] U. Majewska et al. "Trace element concentration distributions in breast, lung and colon tissues". In: *Physics in Medicine and Biology* 52.13 (July 2007). doi = 10.1088/0031-9155/52/13/016, pp. 3895–3911. ISSN: 0031-9155. URL: https://iopscience.iop.org/article/10.1088/0031-9155/52/13/016 (cit. on pp. 9, 10).

[26] M. L. Carvalho, J. Brito, and M. A. Barreiros. "Study of Trace Element Concentrations in Human Tissues by EDXRF Spectrometry". In: *X-Ray Spectrometry* 27.3 (1998). doi = 10.1002/(sici)1097-4539(199805/06)27:3<198::aid-xrs265>3.0.co;2-b, pp. 198–204. ISSN: 00498246 (cit. on p. 9).

[27] M. P. Silva et al. "Determination of Ca, Fe, Cu and Zn and their correlations in breast cancer and normal adjacent tissues". In: *X-Ray Spectrometry* 38.2 (Mar. 2009). doi = 10.1002/xrs.1126, pp. 103–111. ISSN: 00498246. URL: http://doi.wiley.com/10.1002/xrs.1126 (cit. on pp. 9, 43, 45, 49, 51).

[28] M. P. Silva et al. "Trace elements as tumor biomarkers and prognostic factors in breast cancer: a study through energy dispersive x-ray fluorescence". In: *BMC Research Notes* 5.1 (Dec. 2012). doi = 10.1186/1756-0500-5-194, p. 194. ISSN: 1756-0500. URL: https://bmcresnotes.biomedcentral.com/articles/10.1186/1756-0500-5-194 (cit. on pp. 9, 49, 51).

[29] M. Carvalho et al. "Trace elements in human cancerous and healthy tissues: A comparative study by EDXRF, TXRF, synchrotron radiation and PIXE". In: *Spectrochimica Acta Part B: Atomic Spectroscopy* 62.9 (Sept. 2007). doi = 10.1016/j.sab.2007.03.030, pp. 1004–1011. ISSN: 05848547. URL: https://linkinghub.elsevier.com/retrieve/pii/S0584854707001000 (cit. on pp. 9, 10, 49, 51).

[30] A. Wandzilak et al. "X-ray fluorescence study of the concentration of selected trace and minor elements in human brain tumours". In: *Spectrochimica Acta Part B: Atomic Spectroscopy* 114 (Dec. 2015). doi = 10.1016/j.sab.2015.10.002, pp. 52–57. ISSN: 05848547. URL: https://linkinghub.elsevier.com/retrieve/pii/S0584854715002396 (cit. on p. 10).

[31] A. Banas et al. "Correlation of concentrations of selected trace elements with Gleason grade of prostate tissues". In: *JBIC Journal of Biological Inorganic Chemistry* 15.7 (Sept. 2010). doi = 10.1007/s00775-010-0675-5, pp. 1147–1155. ISSN: 0949-8257. URL: http://link.springer.com/10.1007/s00775-010-0675-5 (cit. on p. 10).

[32] P. M. Carvalho et al. "Energy dispersive X-ray fluorescence quantitative analysis of biological samples with the external standard method". In: *Spectrochimica Acta Part B: Atomic Spectroscopy* 174 (2020). doi = 10.1016/j.sab.2020.105991, p. 105991. ISSN: 0584-8547. URL: http://www.sciencedirect.com/science/article/pii/S0584854720304304 (cit. on pp. 10, 44, 48, 50, 52).

[33] A. Kubala-Kukuś et al. "Trace element load in cancer and normal lung tissue". In: *Nuclear Instruments and Methods in Physics Research Section B: Beam Interactions with Materials and Atoms* 150.1-4 (Apr. 1999). doi = 10.1016/S0168-583X(98)01057-X, pp. 193–199. ISSN: 0168583X. URL: https://linkinghub.elsevier.com/retrieve/pii/S0168583X9801057X (cit. on p. 10).

[34] *"R Logo"Accessed February 8, 2021*. URL: https://www.r-project.org/logo (cit. on p. 12).

[35] R Core Team. *R: A Language and Environment for Statistical Computing*. R Foundation for Statistical Computing. Vienna, Austria, 2021. URL: https://www.R-project.org/ (cit. on p. 12).

[36] *"M4 TORNADO | Bruker"Accessed May 18, 2021*. URL: https://www.bruker.com/en/products-and-solutions/elemental-analyzers/micro-xrf-spectrometers/m4-tornado.html (cit. on p. 13).

[37] S. Pessanha et al. “Determination of demineralization depth in tooth enamel exposed to abusive use of whitening gel using micro-Energy Dispersive X ray Fluorescence”. English. In: *Spectrochimica Acta Part B-Atomic Spectroscopy* 138 (Dec. 2017). Portuguese Foundation for Science and Technology (FCT) for the post-doctoral grant with reference SFRH/BPD/94234/2013., pp. 8–13. ISSN: 0584-8547. DOI: 10.1016/j.sab.2017.10.001 (cit. on p. 19).

[38] S. Pessanha et al. “Nondestructive analysis of Portuguese “dinheiros” using XRF: overcoming patina constraints”. English. In: *Applied Physics A-Materials Science & Processing* 119.3 (June 2015). This investigation was funded by Fundacao para a Ciencia e Tecnologia (FCT) with the project Pest-OE/FIS/UI0303/2014. S. Pessanha would like to thank FCT for the postdoc Grant SFRH/BPD/94234/2013. M. E. M. Jorge would like thank project Pest-OE/QUI/UI0612/2013 for the funding., pp. 1173–1178. ISSN: 0947-8396. DOI: 10.1007/s00339-015-9087-2 (cit. on p. 19).

[39] *"NIST - X-Ray Mass Attenuation Coefficients"Accessed May 10, 2021*. URL: https://physics.nist.gov/PhysRefData/XrayMassCoef/tab2.html (cit. on pp. 20, 27).

[40] T. Glover. *Pocket Ref*. 3rd. 2003, p. 324 (cit. on p. 20).

I

Annex 1

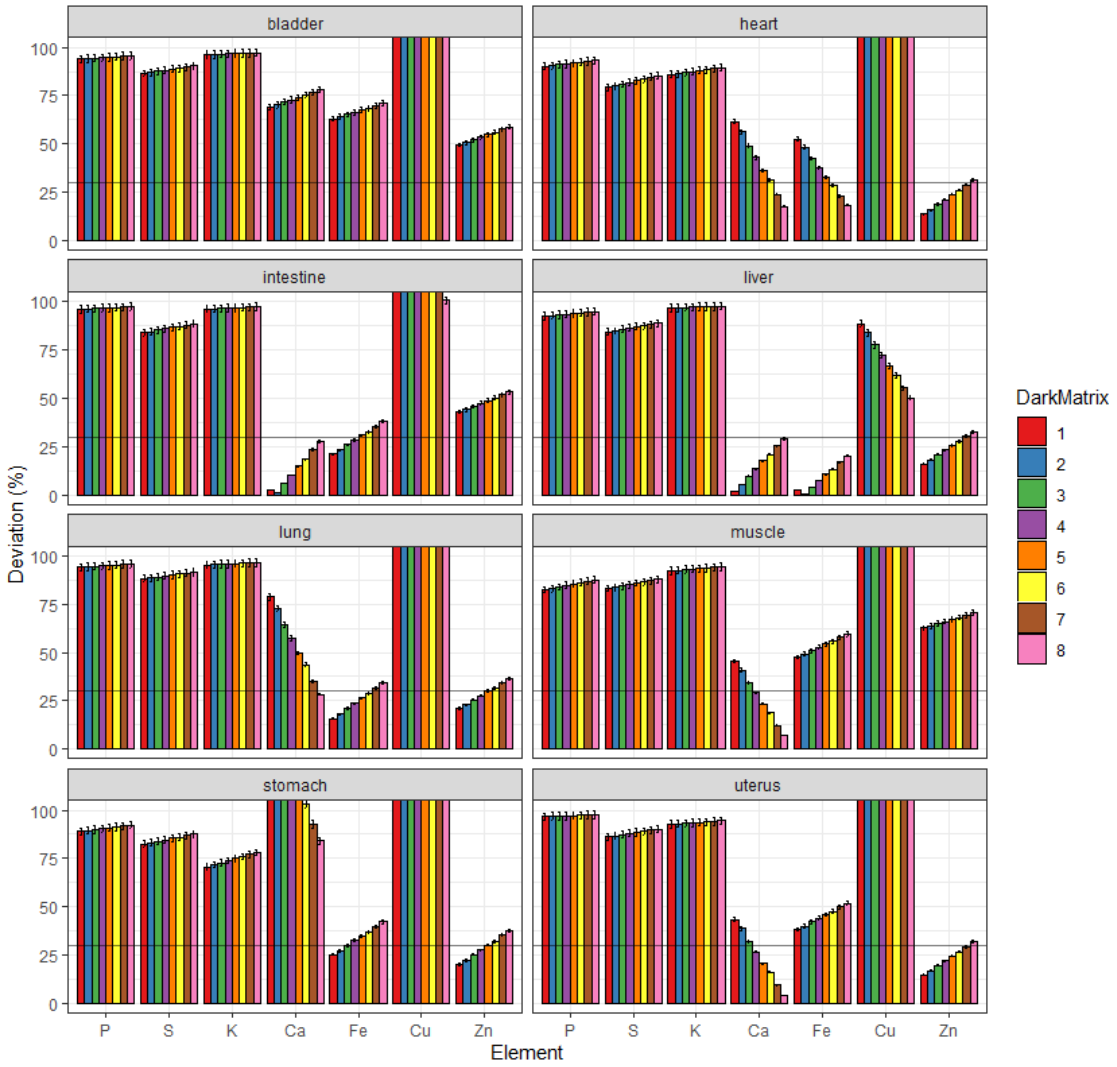

Figure I.1: Deviation of the quantification results of the remaining FFPE samples from reference values (in %).